10280–10296 *Nucleic Acids Research, 2020, Vol. 48, No. 18* *Published online 21 September 2020*
doi: 10.1093/nar/gkaa761

eIF2α interactions with mRNA control accurate start codon selection by the translation preinitiation complex

Anil Thakur[1,2,*], Swati Gaikwad[1], Anil K. Vijjamarri[1] and Alan G. Hinnebusch[1,*]

[1]Division of Molecular and Cellular Biology, *Eunice Kennedy Shriver* National Institute of Child Health and Human Development, NIH, Bethesda, MD 20892, USA and [2]Regional Centre for Biotechnology, 3rd milestone Gurgaon-Faridabad Expressway, Faridabad 121001, India

Received July 21, 2020; Revised August 26, 2020; Editorial Decision August 29, 2020; Accepted September 02, 2020

ABSTRACT

In translation initiation, AUG recognition triggers rearrangement of the 48S preinitiation complex (PIC) from an open conformation to a closed state with more tightly-bound Met-tRNA$_i$. Cryo-EM structures have revealed interactions unique to the closed complex between arginines R55/R57 of eIF2α with mRNA, including the −3 nucleotide of the 'Kozak' context. We found that R55/R57 substitutions reduced recognition of a UUG start codon at *HIS4* in Sui$^-$ cells (Ssu$^-$ phenotype); and *in vitro*, R55G-R57E accelerated dissociation of the eIF2·GTP·Met-tRNA$_i$ ternary complex (TC) from reconstituted PICs with a UUG start codon, indicating destabilization of the closed complex. R55/R57 substitutions also decreased usage of poor-context AUGs in *SUI1* and *GCN4* mRNAs *in vivo*. In contrast, eIF2α-R53 interacts with the rRNA backbone only in the open complex, and the R53E substitution enhanced initiation at a UUG codon (Sui$^-$ phenotype) and poor-context AUGs, while reducing the rate of TC loading (Gcd$^-$ phenotype) *in vivo*. Consistently, R53E slowed TC binding to the PIC while decreasing TC dissociation at UUG codons *in vitro*, indicating destabilization of the open complex. Thus, distinct interactions of eIF2α with rRNA or mRNA stabilize first the open, and then closed, conformation of the PIC to influence the accuracy of initiation *in vivo*.

INTRODUCTION

Accurate identification of the translation initiation codon is critical to ensure the synthesis of the correct cellular proteins in the proper amounts. In eukaryotes, translation initiation generally occurs by a cap-dependent scanning mechanism, wherein the small (40S) subunit of the ribosome recruits methionyl initiator tRNA (Met-tRNA$_i$) in a ternary complex (TC) with GTP-bound eukaryotic initiation factor 2 (eIF2), in a reaction stimulated by factors eIF1, eIF1A and eIF3. The resulting 43S preinitiation complex (PIC) attaches to the capped 5′ end of mRNA and scans the mRNA leader for an AUG start codon. The nucleotide sequence immediately surrounding the start codon—the 'Kozak context'—particularly at the −3 and +4 positions (numbered from the A of AUG (+1)) influences the efficiency of start codon selection. In the scanning PIC, eIF1 and eIF1A promote an open, scanning-conducive conformation of the 40S subunit with TC bound in a relatively unstable conformation, 'P_{OUT}', which facilitates the inspection of successive triplets in the peptidyl (P) decoding site for complementarity with the anticodon of Met-tRNA$_i$. The GTP bound to eIF2 can be hydrolyzed, stimulated by GTPase activating protein eIF5, but eIF1 blocks release of inorganic phosphate (P_i) at non-AUG codons. Start codon recognition triggers dissociation of eIF1 from the 40S subunit, enabling both P_i release from eIF2-GDP·P_i and more stable TC binding to the PIC, with Met-tRNA$_i$ more fully accommodated in a 'P_{IN}' state. The N-terminal domain (NTD) of eIF5 binds to the 40S platform at the position vacated by eIF1 and makes stabilizing interactions with Met-tRNA$_i$ (Figure 1A). Subsequent dissociation of eIF2-GDP and other eIFs from the 48S PIC enables eIF5B-catalyzed subunit joining and formation of an 80S initiation complex ready to commence protein synthesis (1–3).

eIF1 plays a dual role in translation initiation. It promotes the open conformation of the PIC, to which TC rapidly loads in the P_{OUT} conformation, while clashing with Met-tRNA$_i$ in the P_{IN} state. Hence, eIF1 dissociation from the 40S subunit is required for start codon recognition, and mutations that weaken eIF1 binding to 40S subunits confer dual defects *in vivo*: (i) they reduce the rate of TC loading, since eIF1 promotes TC binding to the open conformation of the PIC and (ii) they increase initiation at

*To whom correspondence should be addressed. Tel: +1 301 496 4480; Email: ahinnebusch@nih.gov
Correspondence may also be addressed to Anil Thakur. Email: anil.thakur@rcb.res.in

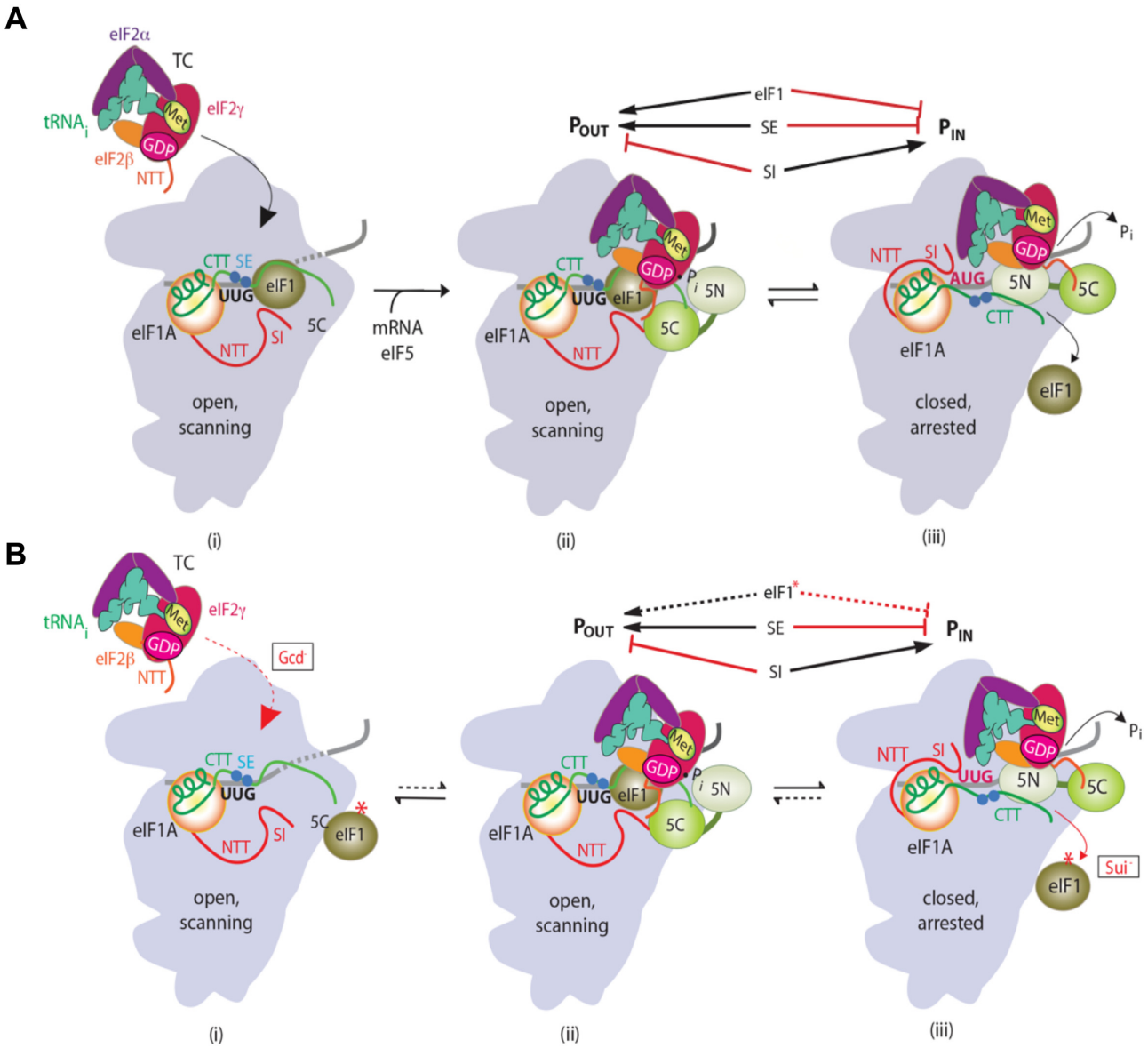

Figure 1. Model describing conformational rearrangements of the PIC during scanning and start codon recognition and the consequences of Sui$^-$ substitutions in eIF1. (**A**) Assembly of the PIC, scanning and start codon selection in WT cells. (i) eIF1 and the scanning enhancer (SE) elements in the CTT of eIF1A stabilize an open conformation of the 40S subunit in the 43S PIC to which TC rapidly loads. (ii) After joining with mRNA and eIF5, the 43S PIC in the open conformation scans the mRNA for the start codon with Met-tRNA$_i$ bound in the P$_{OUT}$ state. The GAP domain in the N-terminal domain of eIF5 (5N) stimulates GTP hydrolysis by the TC to produce GDP-P$_i$, but release of P$_i$ is blocked. The unstructured NTT of eIF2β interacts with eIF1 to stabilize eIF1●40S association in the open PIC conformation. (iii) On AUG recognition, the Met-tRNA$_i$ moves from the P$_{OUT}$ to P$_{IN}$ state, clashing with eIF1. Movement of eIF1 away from the P site disrupts its interaction with the eIF2β-NTT, and the latter interacts with the eIF5-CTD instead. eIF1 dissociates from the 40S subunit, and the eIF1A SE elements move away from the P site. The eIF5-NTD replaces eIF1 on the 40S platform and interacts with the eIF1A CTT, facilitating P$_i$ release, stabilizing Met-tRNA$_i$ binding in the P site, and blocking reassociation of eIF1 with the 40S subunit. The arrows above summarize that eIF1 and the eIF1A SE elements promote P$_{OUT}$ and block the transition to the P$_{IN}$ state, whereas the scanning inhibitor (SI) elements in the NTT of eIF1A stabilize the P$_{IN}$ state. (Adapted from (8,34,35). (**B**) (i) An eIF1 substitution that weakens its binding to the 40S subunit and confers decreased eIF1 occupancy in the 43S PIC decreases the rate of TC loading to confer the Gcd$^-$ phenotype (red dotted arrow). (ii, iii) While the decreased rate of TC loading slows formation of the scanning complex (ii) from the 43S PIC (i), once TC eventually binds and scanning commences, an increased frequency of mutant eIF1 dissociation from the open/P$_{OUT}$ conformation enables more frequent rearrangement to the P$_{IN}$ state at UUG codons (iii), conferring the Sui$^-$ phenotype (red solid line).

near cognate codons or AUG codons in poor context, by destabilizing the open/P_{OUT} state and favoring rearrangement to the closed/P_{IN} state without perfect base pairing of Met-tRNA$_i$ with an AUG start codon (1,2). A reduced rate of TC loading resulting from such eIF1 mutations confers derepressed translation of *GCN4* mRNA *in vivo* (the Gcd$^-$ phenotype), as slower TC binding to PICs scanning the *GCN4* mRNA leader allows inhibitory upstream open reading frames (uORFs) to be bypassed in favor of reinitiation further downstream at the *GCN4* coding sequences (4). Increased initiation at near-cognate codons in such eIF1 mutants restores translation of *his4–303* mRNA, lacking the AUG start codon, by elevating initiation at an in-frame UUG triplet at the third codon (the Sui$^-$ phenotype) (5) (Figure 1B). The AUG codon of the eIF1 gene itself (*SUI1* in yeast) occurs in suboptimal context and the frequency of its recognition is inversely related to eIF1 abundance, establishing a negative feedback loop that maintains proper eIF1 levels (6,7). Whereas overexpressing WT eIF1 suppresses initiation at its own suboptimal AUG codon, eIF1 mutants defective for 40S binding relax discrimination against poor context and increase the translational efficiency of *SUI1* mRNA, elevating expression of such eIF1 variants. Such effects have been attributed to the altered rates of eIF1 dissociation from the scanning PIC, impeding or enhancing, respectively, inappropriate isomerization to the closed state at near-cognate start codons or AUG codons in poor context (8,9). These findings on eIF1 established the Gcd$^-$, Sui$^-$ and Ssu$^-$ phenotypes, and alterations in translation of *SUI1* mRNA and attendant changes in eIF1 expression, as reliable *in vivo* reporters of genetic perturbations in initiation factors that specifically disfavor the open/P_{OUT} or closed/P_{IN} state of the scanning PIC *in vivo* (1,2).

Many mechanistic aspects of the translation initiation process have been illuminated by cryo-electron microscopy (cryo-EM) structures of two distinct partial yeast 48S (py48S) complexes, both containing eIF1, eIF1A, mRNA and TC, but appearing to represent the open, scanning conformation (py48S-open) or a closed conformation arrested at the start codon (py48S-closed) (10). The py48S-open complex exhibits an upward movement of the 40S head away from the body that widens both the mRNA binding cleft and the P site, eliminating certain 40S contacts with the mRNA and Met-tRNA$_i$ that occur only in the py48S-closed complex. Conversely, the closed structure shows a constricted mRNA channel and narrowed P site that fully encases Met-tRNA$_i$. Comparing these two structures has enabled predictions about the factors and specific residues that preferentially stabilize either the open or closed state of the PIC (2,10). These include an electrostatic clash between the β-hairpin loop-2 of eIF1 and the D-loop of Met-tRNA$_i$ that was shown to restrict the P_{OUT} to P_{IN} transition at non-AUG codons and AUGs in poor context (11), a functionally similar clash between eIF2β and Met-tRNA$_i$ (12), physical interactions between eIF1 and eIF2β unique to py48S-open that hold eIF1 and eIF2β in their restrictive positions relative to Met-tRNA$_i$ in the scanning PIC (10,12), interaction of the unstructured N-terminal tail (NTT) of eIF1A with the mRNA and AUG:anticodon duplex unique to py48S-closed that specifically stabilize the P_{IN} state (13), and interactions of the eIF5-NTD with Met-tRNA$_i$ that occur following eIF1 dissociation that stabilize rather than restrict Met-tRNA$_i$ accomodation in the P_{IN} state following AUG selection (3).

The -3 nucleotide is the most influential residue of the Kozak context, with a purine (usually an A) enhancing AUG selection in mammals (14). In budding yeast, 5′ UTRs are highly biased for A's from positions −1 to −30, with a particularly strong preference at position −3 comparable to that in mammals. Mutational analysis showed that sequence context regulates initiation efficiency in yeast, with an A at −3 conferring the greatest stimulation; although the dynamic range of context effects appears to be smaller in yeast than in mammals, at least for AUG start codons (15). The importance of an A at −3 in both yeast and mammals suggests that this residue makes a conserved interaction with an initiation factor or ribosomal constituent located near the ribosomal E site, where the −3 nucleotide is positioned when AUG occupies the P site, to enhance the formation or stability of the 48S PIC. Biochemical evidence suggested that interaction of eIF2α with the −3 nucleotide mediates the stimulatory effect of a purine at that position on AUG selection in reconstituted mammalian 48S PICs (16); however, *in vivo* evidence for this hypothesis is lacking.

Examining the structures of the py48S-open and py48S-closed complexes reveals that all three domains of eIF2α (D1–D3) interact extensively with different regions of Met-tRNA$_i$ in both complexes (Figure 2A and B). In the transition from the open to closed state, the positions of the three domains are slightly altered with respect to one another, to Met-tRNA$_i$, and to other components of the PIC. In particular, movement of D-1 positions Arg residues R55 and R57, present in the extended loop in D-1, to interact with the −3 and −2 nucleotides in mRNA, respectively (10) (Figure 2A and B). Being restricted to the closed complex, these interactions might be expected to preferentially stabilize the P_{IN} state, and perhaps mediate the stimulatory effect of A at −3 on initiation frequency. Accordingly, we have examined the effects of substitutions of eIF2α R55 and R57 on the ability to discriminate between poor and weak Kozak contexts, and between AUG and near-cognate (e.g. UUG) start codons. Our findings do not support the hypothesis that the contacts of these residues with mRNA underlie the stimulatory effect of preferred Kozak context in yeast cells. Rather, these contacts appear to be crucial for recognition of poor initiation sites, including AUGs in poor context and near-cognate start codons, suggesting that they represent another molecular interaction that specifically stabilizes the closed conformation of the PIC. As such, they are particularly important for utilization of suboptimal start codons that assemble 48S PICs of inherently lower stability compared to AUGs in optimum context.

MATERIALS AND METHODS

Plasmid and yeast strain constructions

Yeast strains used in this study are listed in Supplementary Table S2. Strains ATY201 to ATY211 and ATY113 to ATY215, harboring mutant *SUI2* alleles on single copy (sc) *LEU2* plasmids were derived from strain H2507 (*MATa ura3-52 leu2-3, leu2-112 trp1Δ-63 sui2Δ gcn2Δ* p919 [*URA3 SUI2*]) by plasmid shuffling, using growth on 5-fluoorotic

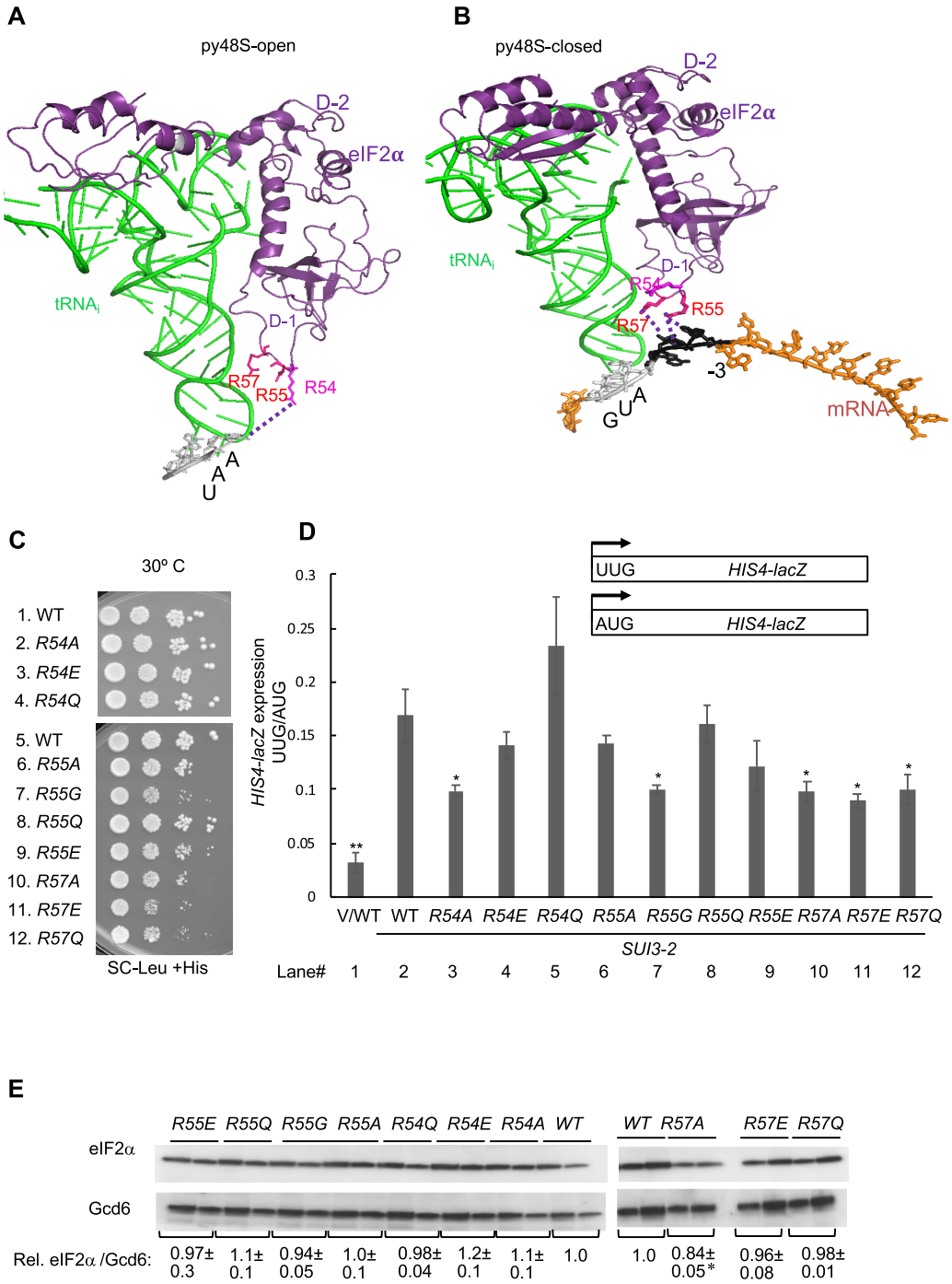

Figure 2. Substitutions in the eIF2α-D1 loop increase discrimination against UUG start codons *in vivo*. (**A**, **B**) Cryo-EM structures of the py48S PIC showing contacts between eIF2α-D1 and mRNA in the py48S-open state (A) and py48S closed state (B). eIF2α is shown in purple with the key Arg residues in the D-1 loop shown as sticks in magenta, mRNA in orange with the AUG in gray and Kozak nucleotides in black, and Met-tRNA$_i$ in green (10). (**C**) Ten-fold serial dilutions of *sui2Δ* strain H2507 derivatives containing the indicated *SUI2* alleles were spotted on synthetic complete medium lacking leucine (SC-Leu) and incubated at 30°C for 2 days. All images derive from results obtained in parallel. (**D**) *HIS4-lacZ* reporters with UUG or AUG start codons were assayed to calculate UUG:AUG initiation ratios. Derivatives of H2507 containing the indicated *SUI2* alleles in the presence of the dominant *SUI3–2* allele on the *TRP1* plasmid p4280, each harboring the appropriate *HIS4-lacZ* reporter plasmid, were cultured in synthetic dextrose minimal medium (SD) at 30°C to A_{600} of ∼1.0, and β-galactosidase activities (in units of nanomoles of *o*-nitrophenyl-β-D-galactopyranoside cleaved per min per mg) were measured in whole cell extracts (WCEs). The ratio of expression of the UUG to AUG reporter was calculated from four to six different transformants, and the mean and SEMs were plotted. Asterisks indicate significant differences between mutant and WT as judged by a two-tailed, unpaired Student's *t*-test (*$P < 0.05$; **$P < 0.01$). (**E**) Derivatives of H2507 containing the indicated *SUI2* alleles were cultured in SD supplemented with Trp and Ura at 30°C to A_{600} of ∼1.0, and WCEs were subjected to western blot analysis using antibodies against eIF2α and Gcd6 (as loading control). The band intensities were quantified by scanning densitometry using NIH ImageJ software for eIF2α and Gcd6, and the eIF2α/Gcd6 ratios calculated from multiple replicate cultures. Mean ratios and SEMs are shown. The asterisk indicates a significant difference between the *R57A* mutant and WT ratios as judged by a two-tailed, unpaired Student's *t*-test (*$P < 0.05$).

acid (5-FOA) medium to select for loss of *URA3* plasmid p919 containing WT *SUI2* (plasmid-shuffling). The QuikChange site-directed mutagenesis system (Stratagene) was employed with the primers indicated in Supplemental Table S3 to generate all mutant *SUI2* plasmids listed in Supplemental Table S1, using as templates plasmids pC171 for yeast plasmids. Strains ATY218 to ATY220 used for purification of eIF2 variants containing eIF2-R55G-R57E, R55G-R57Q and R53E, respectively, were constructed from H3840 by plasmid shuffling to replace pAV1089 (containing *URA3* and WT *SUI2)* with high-copy *LEU2* plasmids containing the appropriate *SUI2* alleles derived from pAV1726 by site-directed mutagenesis, as described above (Supplementary Table S1).

Biochemical assays using yeast cell extracts

Assays of β-galactosidase activity in whole cell extracts (WCEs) were performed as described previously (17). For western analysis, WCEs were prepared by trichloroacetic acid extraction as previously described (18) and immunoblot analysis was conducted as previously described (19) using antibodies against eIF1/Sui1 (20) and Hcr1 (20). Enhanced chemiluminiscence (Amersham) was used to visualize immune complexes, and signal intensities were quantified by densitometry using NIH ImageJ software.

Biochemical analysis in the reconstituted yeast system

WT eIF2 and eIF2 variants were overexpressed in yeast and purified as described (21). 40S subunits were purified as described previously from strain YAS2488 (21). WT eIF1 and eIF1A were expressed in bacterial strain BL21(DE3) Codon Plus cells (Agilent Technologies) and purified using the IMPACT system (New England Biolabs) as described previously (21). Model mRNAs with sequences 5′-GGAA[UC]$_7$UAUG[CU]$_{10}$C-3′ and 5′-GGAA[UC]$_7$UUUG[CU]$_{10}$C-3′were purchased from Thermo Scientific. Yeast tRNA$_i^{Met}$ was synthesized from a hammerhead fusion template using T7 RNA polymerase, charged with [^{35}S]-methionine, and used to prepare radiolabeled eIF2·GDPNP·[^{35}S]-Met-tRNA$_i$ ternary complexes ([^{35}S]-TC), all as previously described (21). Charged, unlabeled yeast Met-tRNA$_i^{Met}$ was purchased from tRNA Probes, LLC.

TC dissociation rate constants (k_{off}) were measured by monitoring the amount of [^{35}S]-TC that remains bound to 40S·eIF1·eIF1A·mRNA (43S·mRNA) complexes over time, in the presence of excess unlabeled TC (chase), using a native gel shift assay to separate 40S-bound from unbound [^{35}S]-TC. 43S·mRNA complexes were preassembled for 2 h at 26°C in reactions containing 40S subunits (20 nM), eIF1A, eIF1, eIF5-G31R (1 μM) (where indicated), mRNA (10 μM) and [^{35}S]-TC (pre-assembled from 0.25 μM eIF2 (WT or mutant variants), 0.1 mM GDPNP, and 1 nM [^{35}S]-Met-tRNA$_i$) in 60 μl of reaction buffer (30 mM HEPEs–KOH (pH 7.4), 100 mM potassium acetate (pH 7.4), 3 mM magnesium acetate and 2 mM dithiothreitol). To initiate each dissociation reaction, a 6 μl-aliquot of the preassembled 43S·mRNA complexes was mixed with 3 μl of 3-fold concentrated unlabeled TC chase (comprised of 2 μM WT eIF2, 0.3 mM GDPNP and 0.9 μM Met-tRNA$_i$), representing a 300-fold excess over labeled TC in the final dissociation reaction, and incubated for the prescribed period of time. A converging time course was employed so that all dissociation reactions were terminated simultaneously by the addition of native-gel dye and loaded directly on a running native gel. The fraction of [^{35}S]-Met-tRNA$_i$ remaining in 43S complexes at each time point was determined by quantifying the 40S-bound and unbound signals by Phosphor Imaging, normalized to the ratio observed at the earliest time-point; and the data were fit with a single exponential equation (22).

TC association rates were measured by mixing [^{35}S]-TC with 40S·eIF1·eIF1A·mRNA complexes and quenching the binding reaction at various times by adding a 300-fold excess of unlabeled WT TC. Reactions were assembled as described above using 6 μl of sample and 3 μl of chase, and completed reactions were mixed with 2 μl of native gel dye before resolving 10 μl by native gel electrophoresis. As above, samples were loaded within minutes of one another on a running native gel. The k_{obs} values were calculated by plotting the fraction of [^{35}S]-Met-tRNA$_i$ bound to 40S·eIF1·eIF1A·mRNA complexes against time and fitting the data with a single exponential equation. The resulting k_{obs} values were plotted against the 40S subunit concentrations used in different experiments and the data were fit to a straight line. The slopes of these lines correspond to the second-order rate constants (k_{on}) for TC binding.

RESULTS

Substitutions of R55 and R57 in the eIF2α-D1 loop increase discrimination against UUG start codons *in vivo*

Comparing the cryo-EM structures of the py48S-open and py48S-closed complexes reveals contacts between eIF2α-D1 residues R55 and R57 with the nucleotides immediately upstream of the AUG start codon that are restricted to the closed complex (Figure 2A and B). The adjacent residue R54 comes close to the mRNA in the open complex but is distant in the closed state, and hence might play a role in specifically stabilizing the open, scanning complex. To examine their possible roles in recognition of the start codon and Kozak context *in vivo*, we made mutations affecting each of these Arg residues, substituting them with Gly or Ala to eliminate or minimize their side-chains, with Gln to eliminate their charge, or with Glu to replace their positive charge with negative charge. Plasmid-shuffling (23) was employed to replace a plasmid-borne WT allele of the *SUI2* gene encoding eIF2α with mutant *SUI2* alleles encoding the desired variants in a strain lacking chromosomal *SUI2*.

Substituting R55 with Gly or Glu, and R57 with Ala, Glu or Gln, conferred noticeable slow growth phenotypes (Slg$^-$) on synthetic complete medium, whereas neither Ala, Glu or Gln substitutions of R54 affected cell growth (Figure 2C) (These phenotypes, and various others determined below for the different eIF2α substitutions, are summarized in Supplementary Table S4). Western analysis of whole cell extracts (WCEs) of the mutant strains using antibodies against eIF2α showed that, with the exception of small ∼20% increases or decreases in the steady state level of eIF2α conferred by R54E and R57A, respectively, all of

the other variants were expressed at levels indistinguishable from WT eIF2α (Figure 2E). Thus, it appears that R55 and R57 substitutions primarily reduce the function, not expression, of eIF2α.

Previously, it was found that perturbing interactions within the PIC restricted to the closed conformation increases discrimination against near-cognate UUG start codons, suppressing the elevated UUG initiation conferred by Sui⁻ mutations in other initiation factors to confer the Ssu⁻ phenotype (1,2). Hence, we began by assaying the *SUI2* mutations for reductions in expression of a *HIS4-lacZ* fusion with a UUG start codon in comparison to the matched AUG-initiated *HIS4-lacZ* reporter in cells harboring the dominant *SUI3–2* allele, encoding the eIF2β-S264Y variant that elevates the UUG:AUG *HIS4-lacZ* initiation ratio in cells also expressing WT eIF2β (24). As expected, the UUG:AUG ratio in the *SUI3-2* strain containing WT *SUI2* was >5-fold higher than the ratio of ∼0.03 measured in the isogenic WT *SUI2* strain lacking *SUI3-2* (Figure 2D, cols. 1–2). Interestingly, the *R54A, R55G* and all three substitutions of R57 (*R57A, R57E,*- and *R57Q*) conferred significant reductions in the UUG:AUG ratio in the presence of *SUI3–2* compared to that measured in the WT *SUI2* strain (Figure 2D, cols. 3, 7, 10–12 versus 2) (Supplementary Table S4). As frequently found for Ssu⁻ substitutions (8,25–27) none of these five *SUI2* alleles significantly altered the UUG:AUG ratio in cells lacking *SUI3-2* (Supplementary Figure S1, cols. 2, 6, 9–11 versus 1), whereas *R54Q* conferred a small increase in the UUG:AUG ratio, indicating a weak Sui⁻ phenotype for this substitution (Supplementary Figure S1, col. 4 versus 1) (Supplementary Table S4). Thus, R54A, R55G, and all three substitutions of R57 confer Ssu⁻ phenotypes, suggesting specific destabilization of the closed PIC conformation *in vivo*.

To provide additional support for this last conclusion, we determined whether combining the eIF2α R55G substitution with R57E or R57Q would yield a stronger Ssu⁻ phenotype than observed for the corresponding single substitutions. Indeed, both the R55G/R57E and R55G/R57Q double substitutions conferred greater decreases in the *HIS4-lacZ* UUG:AUG initiation ratio in the presence of *SUI3–2* compared to the corresponding single substitutions (Figure 3A, cols. 6–7 versus 3–5 & 2). We also examined the ability of these *SUI2* mutations to suppress the Sui⁻ phenotype conferred by the dominant Sui⁻ allele *SUI5,* encoding the eIF5-G31R variant (24). As expected, introducing *SUI5* into WT *SUI2* cells confers a large, ∼7-fold increase in the UUG:AUG ratio (Figure 3B, col. 2 versus 1). Importantly, the *R55G, R57E* and *R57Q* mutations in *SUI2* significantly reduced this ratio in cells containing *SUI5*, and even greater reductions were seen for the *R55G/R57E* and *R55G/R57Q* double mutants (Figure 3B, cols. 6–7 versus 3–5 & 2) (Supplementary Table S4). Thus, both *SUI2-R55G/R57E* and *SUI2-R55G/R57Q* confer marked Ssu⁻ phenotypes in cells containing either the dominant *SUI3-2* or *SUI5* Sui⁻ alleles.

Previously, we showed that Ssu⁻ substitutions in eIF1 (6) and ribosomal proteins uS7 (26) and uS3 (27) all suppress the growth defect conferred by *SUI5* in addition to mitigating the increased UUG initiation conferred by this dominant Sui⁻ mutation of eIF5. We made the same observation here for *R55G/R57E, R55G/R57Q,* and the corresponding single mutations of *SUI2*, all of which increase the ability of cells also harboring *SUI5* to grow on complete medium at 37°C (Figure 3C, rows 3–7 versus 2).

Interestingly, we noticed that *SUI3-2* can effectively suppress the Slg⁻ phenotypes conferred by the *SUI2* alleles *R55G, R57E, R57Q* and the corresponding double mutations *SUI2-R55G/R57E* and *SUI2-R55G/R57Q* (cf. rows 4, 6, & 8 versus 3, 5 & 7 in Figure 3D and E). One way to explain this observation would be to propose that the *SUI2* Ssu⁻ mutations alter the translation of one or more mRNAs encoding proteins critical for cell growth by increasing discrimination against suboptimal initiation codons, and that the Sui⁻ *SUI3-2* mutation mitigates these effects on the stringency of start codon selection. Regardless of the actual mechanism, these findings provide additional genetic evidence that the Ssu⁻ *SUI2* mutations and the Sui⁻ *SUI3–2* mutations have opposing effects on the transition from open to closed states at suboptimal start codons.

Neither the *SUI2-R55G/R57E* nor *SUI2-R55G/R57Q* mutations substantially change the steady-state levels of eIF2α (Figure 3F), indicating that their ability to suppress phenotypes of *SUI3-2* and *SUI5* derives from altered function, rather than altered expression, of eIF2α.

Ssu⁻ substitutions of R55 and R57 in the eIF2α-D1 loop increase discrimination against AUG codons in suboptimal context

We next addressed whether the eIF2α Ssu⁻ substitutions decrease recognition of AUG start codons in poor Kozak context in parallel with conferring decreased initiation at a UUG start codon, as these phenotypes have been linked previously for Ssu⁻ mutations in eIF1 and eIF1A (6). We first examined the effects of the *SUI2* mutations on expression of eIF1, as the AUG codon of *SUI1* mRNA encoding eIF1 resides in poor context, and WT eIF1 discriminates against this suboptimal context to negatively autoregulate its cellular abundance (6,7). Furthermore, Ssu⁻ mutations in eIF1 and eIF1A were found to increase discrimination against the poor AUG context of *SUI1* mRNA and thereby lower the steady-state levels of eIF1, overcoming the autoregulatory mechanism (6).

Western analysis of WCEs using antibodies against eIF1 revealed significantly reduced eIF1 expression conferred by all five Ssu⁻ alleles of *SUI2* described above in comparison to WT *SUI2*, as shown for *R54A* and *R55G* in Figure 4A (cols. 2 & 6 versus 1) and for *R57A, R57Q* and *R57E* in Figure 4B (cols. 4–6 versus 7). In this assay, the *R54E* and *R55A* mutations also significantly reduced eIF1 expression (Figure 4A, rows 3 & 5 versus 1). Moreover, the *R55G/R57Q* and *R55G/R57E* double mutations conferred stronger reductions in eIF1 levels compared to the corresponding single mutations, with the greatest reduction among all of the mutants observed for *R55G/R57E* (Figure 4B, rows 1 & 3 versus 2, 4–5) (Supplementary Table S4). These results suggest that the Ssu⁻ substitutions in eIF2α increase discrimination against the poor context AUG start codon of *SUI1* mRNA.

Supporting this inference, the *SUI2-R55G/R57E* and *SUI2-R55G/R57Q* double mutations and the correspond-

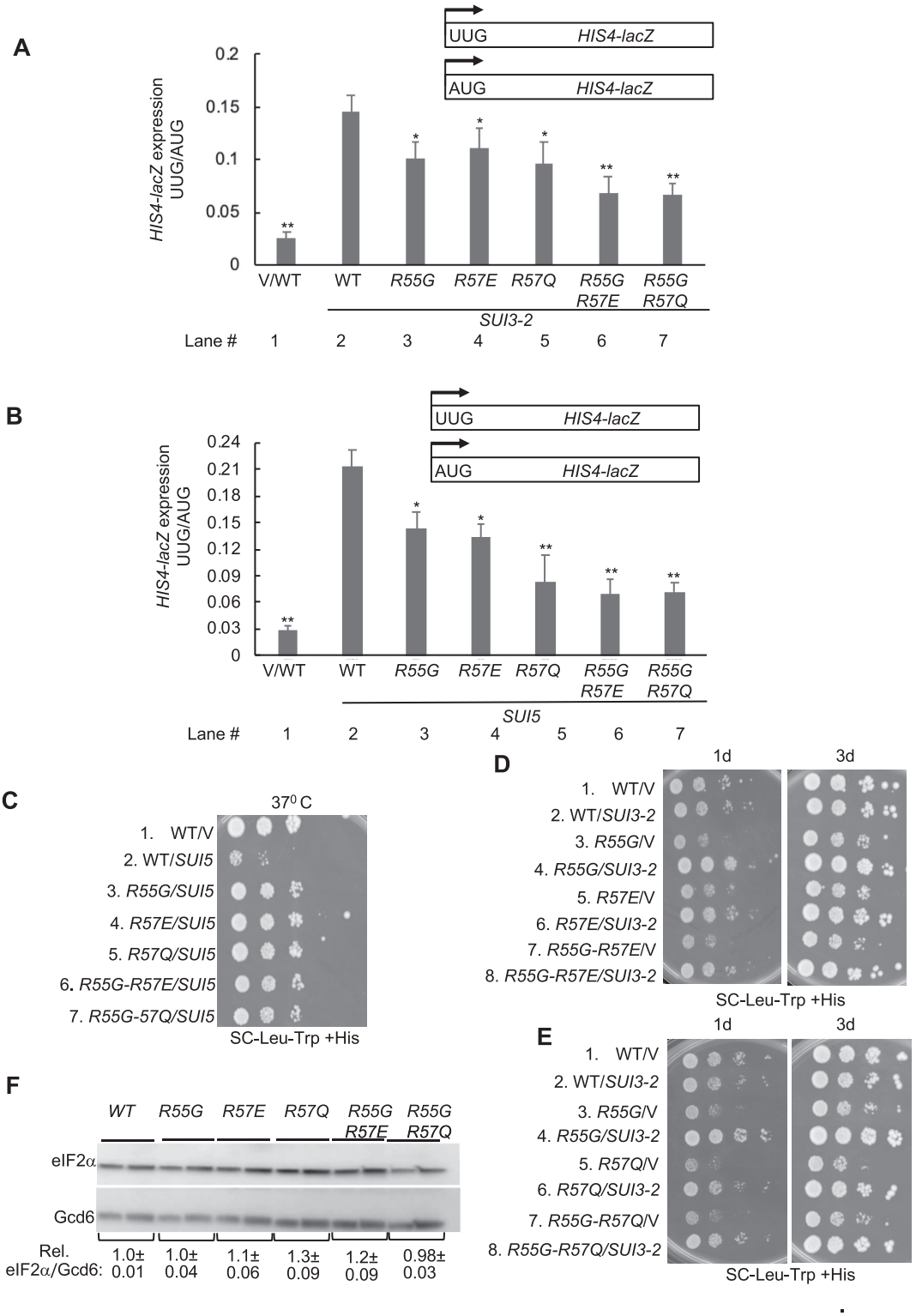

Figure 3. Double substitutions of eIF2α-R55/R57 confer markedly increased discrimination against UUG start codons *in vivo*. (**A**, **B**) Derivatives of *sui2Δ* strain H2507 containing the indicated *SUI2* alleles, each harboring the appropriate *HIS4-lacZ* reporters with UUG or AUG start codons, were assayed to calculate UUG:AUG initiation ratios in the presence of dominant allele *SUI3–2* on plasmid p4280 (A) or *SUI5* on plasmid p4281 (B), all conducted as in Figure 2D. Asterisks indicate significant differences between mutant and WT as judged by a two-tailed, unpaired Student's *t*-test (**P* < 0.05; ***P* < 0.01). (**C**) Ten-fold serial dilutions of H2507 derivatives with the indicated *SUI2* alleles in the presence of dominant *SUI5* on plasmid p4281 were spotted on synthetic complete medium lacking Leu and Trp (SC-Leu-Trp) and incubated at 30°C for 3 days. (**D**, **E**) Ten-fold serial dilutions of H2507 derivatives with the indicated *SUI2* alleles in the presence of dominant *SUI3–2* on plasmid p4280 or vector YCplac22 were spotted on SC-Leu-Trp and incubated at 30°C for 1–3 days. (**F**) Derivatives of *sui2Δ* strain H2507 containing the indicated *SUI2* alleles were cultured in SD supplemented with Trp and Ura at 30°C to A_{600} of ∼1.0, and WCEs were subjected to western blot analysis using antibodies against eIF2α and Gcd6, as described in Figure 2E.

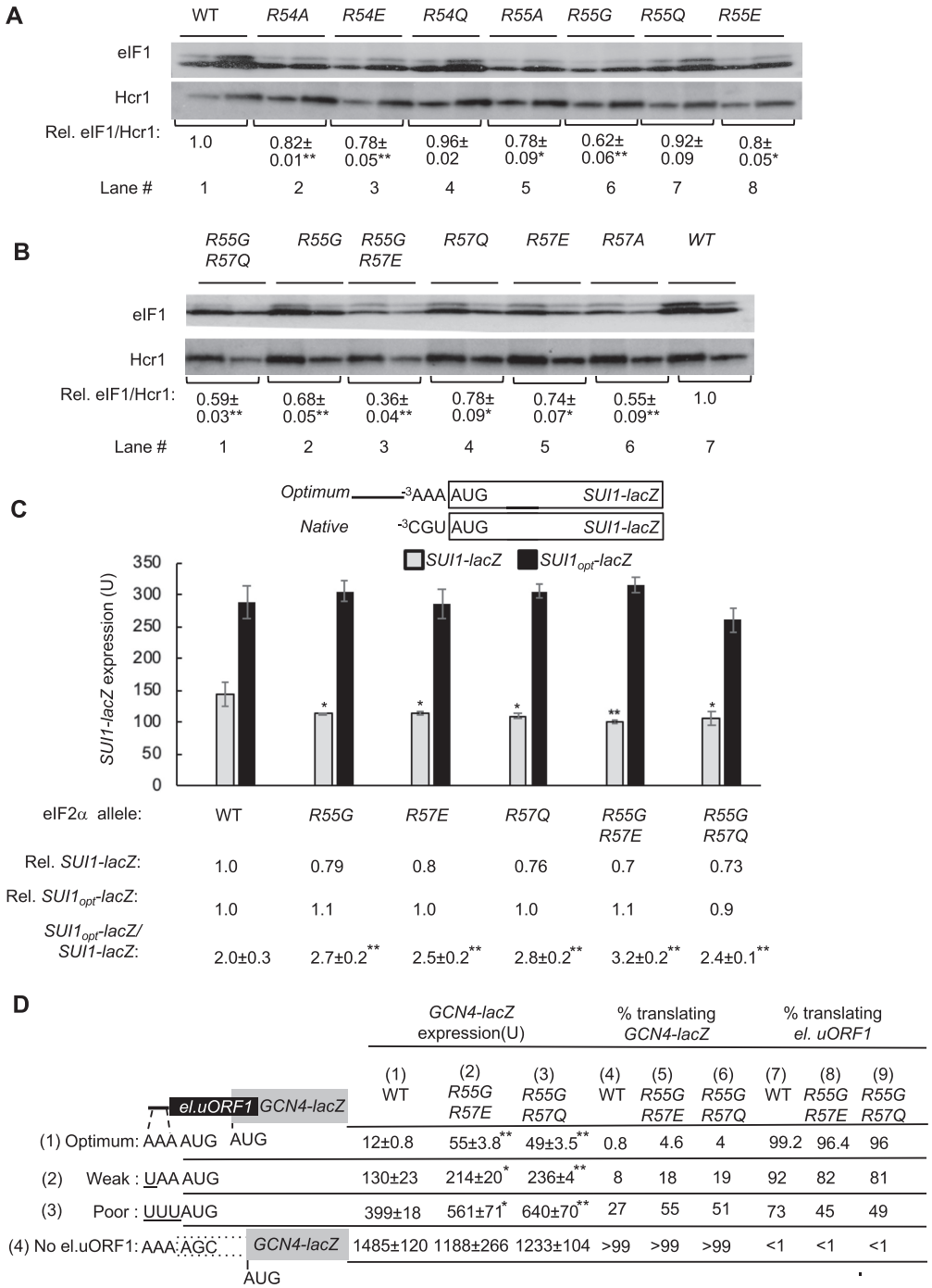

Figure 4. Ssu$^-$ substitutions of R55 and R57 in the eIF2α-D1 loop increase discrimination against AUG codons in suboptimal context. (**A**, **B**) Derivatives of *sui2Δ* strain H2507 containing the indicated *SUI2* alleles were cultured in SD supplemented with Trp and Ura at 30°C to A_{600} of ∼1.0, and WCEs were subjected to western blot analysis using antibodies against eIF1 and Hcr1 (as loading control). Two amounts of each extract differing by a factor of two were loaded in successive lanes. eIF1 western signals were normalized to those for Hcr1 and mean values (±SEM) were calculated from 3 to 4 biological replicates. (**C**) Derivatives of *sui2Δ* strain H2507 containing the indicated *SUI2* alleles but harboring sc plasmids (pPMB24 or pPMB25) with *SUI1-lacZ* fusions with native suboptimal ($_{-3}$CGU$_{-1}$) or optimum ($_{-3}$AAA$_{-1}$) AUG contexts were cultured and assayed for β-galactosidase activities as in Figure 2D. Mean expression levels and SEMs were calculated from six transformants, and relative (Rel.) mean expression levels normalized to that of the WT strain are listed below, along with expression ratios for the *SUI1-lacZ* versus *SUI1-opt-lacZ* reporters. (**D**) Transformants of H2507 harboring WT *SUI2*, *sui2-R55G-R57E* or *sui2-R55G-R57Q* and el.uORF1 *GCN4-lacZ* reporters (pC3502, pC3503 or pC4466) containing the depicted optimum (row 1), weak (row 2) or poor (row 3) context of uAUG-1, or an uORF-less *GCN4-lacZ* reporter with a mutated uAUG-1 (pC3505, row 4), were assayed for β-galactosidase activities as in Figure 2D. Mean expression values with SEMs were determined from six transformants (columns 1, 2 and 3). The percentages of scanning ribosomes that translate el.uORF1 (columns 7, 8 and 9) or leaky-scan uAUG-1 and translate *GCN4-lacZ* instead (columns 4, 5 and 6) were calculated from results in columns 1, 2 and 3 by comparing the amount of expression observed for each uORF-containing reporter to the uORF-less construct, as described in Supplementary Figure S2A–C. (A–D) Asterisks indicate significant differences between mutant and WT as judged by a two-tailed, unpaired Student's *t*-test (*$P < 0.05$; **$P < 0.01$).

ing single mutations all decrease expression of a *SUI1-lacZ* fusion containing the native, poor context of the *SUI1* AUG codon ($_{-3}$CGU$_{-1}$), but not that of a modified fusion (dubbed *SUI1$_{opt}$-lacZ*) containing optimum upstream context ($_{-3}$AAA$_{-1}$) (28). In WT *SUI2* cells, the *SUI1$_{opt}$-lacZ* fusion is expressed at 2-fold higher levels than the native *SUI1-lacZ* fusion, to yield a *SUI1$_{opt}$-lacZ:SUI1-lacZ* expression ratio of 2.0 (Figure 4C, col. 1). The *SUI1$_{opt}$-lacZ:SUI1-lacZ* expression ratio is significantly increased by *R55G/R57E, R55G/R57Q, R55G, R57E,* and *R57Q,* with the largest increase observed for the *R55G/R57E* double mutation (Figure 4C, cols. 2–6 versus 1), which also produced the largest reduction in native eIF1 expression (Figure 4B) (Supplementary Table S4). Thus, these *SUI2* mutations appear to reduce eIF1 expression specifically by increasing discrimination against the native, poor context of the *SUI1* AUG codon.

To provide further evidence that the Ssu$^-$ *SUI2* mutations increase discrimination against AUGs in poor context, we asked whether they decrease initiation at the AUG codon of an upstream ORF in suboptimal context, and thereby increase expression of the downstream ORF encoded on the same mRNA by enhancing 'leaky scanning' past the upstream AUG. To this end, we assayed expression of *GCN4-lacZ* reporters containing a single, modified version of upstream ORF1 elongated to overlap the *GCN4* main ORF (el.uORF1). With the WT optimal context for el.uORF1 of $_{-3}$AAA$_{-1}$, virtually all scanning ribosomes recognize its AUG codon (uAUG-1) and, because reinitiation at the downstream *GCN4* ORF following el.uORF1 translation is essentially nil, *GCN4-lacZ* expression is extremely low (29). In WT cells, replacing only the optimal A with U at the –3 position of el.uORF1 increases leaky scanning of uAUG-1 to produce an ∼11-fold increase in *GCN4-lacZ* translation; introducing the poor context of $_{-3}$UUU$_{-1}$ further increases leaky scanning for an ∼33-fold increase in *GCN4-lacZ* expression, and eliminating uAUG-1 altogether increases *GCN4-lacZ* expression the most, by ∼120-fold (Figure 4D, col. 1, rows 1–4). From these results, the percentages of scanning ribosomes that either translate el.uORF1, or leaky-scan past uAUG-1 and translate *GCN4-lacZ* instead, can be calculated, revealing that >99%, ∼92% and ∼73% of scanning ribosomes recognize uAUG-1 in optimum, weak, and poor context, respectively, in WT cells (Figure 4D, col. 7 (WT), rows 1–4); and accordingly, <1%, ∼8%, ∼27% and >99% initiate at the *GCN4* AUG instead (Figure 4D, col, 4 (WT), rows 1–4). The *GCN4-lacZ* expression and the calculated percentages of ribosomes initiating at the el.uORF1 or *GCN4-lacZ* in WT cells are also plotted in Supplementary Figure S2A–C (WT data).

Subjecting the two *SUI2* double mutants to this analysis revealed that they decrease initiation at uAUG-1, as indicated by significantly increased *GCN4-lacZ* expression for the reporters containing el.uORF1, with either optimum, weak or poor context, but not for the uORF-less reporter (Figure 4D, cf. cols. 2–3 versus 1, rows 1–4; see Supplementary Figure S2A for statistical analysis of *GCN4-lacZ* expression differences between WT and mutants for each reporter). Calculating the percentages of ribosomes that recognize uAUG-1 revealed that both mutations confer a substantial decrease in recognition of uAUG-1 for the poor-context (UUU) reporter, reducing it from ∼73% to ∼45–49% (Figure 4D cols. 8–9 versus col. 7, row 3). The mutations confer a proportionately smaller decrease in uAUG-1 recognition for the weak-context (UAA) reporter, from ∼92% to ∼81–82% (Figure 4D, cf. cols. 8–9 versus col. 7, row 2); and an even smaller decrease for the optimum-context (AAA) reporter, from ∼99.2% to ∼96.4–96% (Figure 4D, cols. 8–9 versus col. 7, row 1). The greater fold-effects of these mutations on recognition of uAUG-1 in poor versus weak, and weak versus optimum contexts, is shown graphically in Supplementary Figure S2B. These findings support the conclusion that the *SUI2* double mutations discriminate against uAUG-1 in suboptimal contexts.

In summary, the foregoing genetic analysis of eIF2α-D1 loop residues supports predictions based on structural comparisons of py48S-open and py48S-closed complexes (Figure 2A, B), that the mRNA contacts made by R55 and R57 exclusively in the closed state participate in preferentially stabilizing this conformation of the PIC on start codon recognition, such that perturbing these interactions decreases utilization of poor start codons, including near-cognate UUG codons and AUG codons in poor context (Supplementary Table S4). While residue R54 does not contact the mRNA in either state (Figure 2A), its greater proximity in the open complex suggested that it might stabilize this conformation instead. However, the increased discrimination against UUG and the poor-context AUG in *SUI1* mRNA observed for various R54 substitutions (Figures 2D and 4A; Supplementary Table S4) suggests the alternative interpretation that R54 substitutions can alter the conformation of nearby R55 and R57 in the eIF2α-D1 loop to diminish the ability of the latter residues to interact productively with mRNA and specifically stabilize the closed PIC conformation.

Ssu$^-$ substitutions of R55 and R57 in the eIF2α-D1 loop diminish Met-tRNA$_i$ accommodation in the P$_{IN}$ state *in vitro*

The genetic data above indicated that the eIF2α double substitutions R55G/R57E and R55G/R57Q increase discrimination against UUG start codons and AUGs in poor context. To provide biochemical evidence that these substitutions impede isomerization to the closed/P$_{IN}$ state, we measured their effects on the rate of TC dissociation from PICs reconstituted from purified components *in vitro.* Partial 43S·mRNA PICs were formed by incubating TCs preassembled with eIF2 (purified from yeast containing WT or mutant eIF2α subunits), [^{35}S]-Met-tRNA$_i$ and nonhydrolyzable GTP analog (GDPNP), with 40S subunits, saturating concentrations of WT or mutant eIF1, WT eIF1A, and an uncapped, unstructured model mRNA containing either an AUG or a UUG start codon (mRNA(AUG) or mRNA(UUG)). The pre-assembled 43S·mRNA PICs were incubated with a chase of excess unlabeled WT TC for increasing time-periods, and the fraction of [^{35}S]-labeled TC remaining bound to the PIC was quantified after resolving 40S-bound and unbound fractions via native gel electrophoresis, from which the rate of dissociation (k_{off}) was calculated (Figure 5A and Supplementary Figure S4A). Previous work has indicated that TC bound in the open/P$_{OUT}$ conformation is unstable during electrophoresis

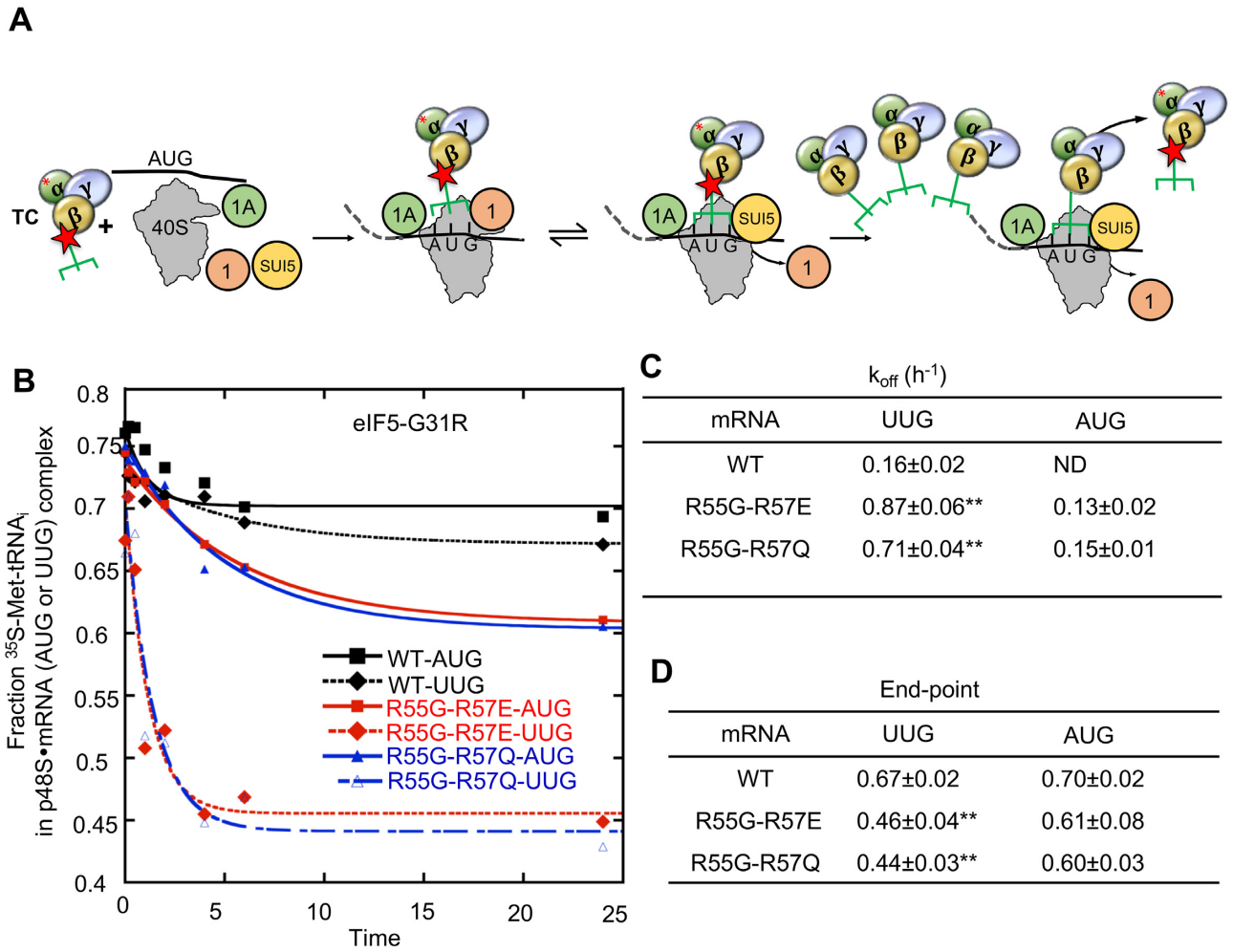

mRNA	UUG	AUG
WT	0.16±0.02	ND
R55G-R57E	0.87±0.06**	0.13±0.02
R55G-R57Q	0.71±0.04**	0.15±0.01

mRNA	UUG	AUG
WT	0.67±0.02	0.70±0.02
R55G-R57E	0.46±0.04**	0.61±0.08
R55G-R57Q	0.44±0.03**	0.60±0.03

Figure 5. Ssu$^-$ substitutions of R55 and R57 in the eIF2α-D1 loop diminish Met-tRNA$_i$ accommodation in the P$_{IN}$ state *in vitro.* (**A**) Measurement of TC dissociation kinetics. Partial 48S complexes were assembled with radiolabeled TCs assembled with [^{35}S]-Met-tRNA$_i$ and eIF2 containing either WT or mutant eIF2α subunits, eIF1, eIF1A, model mRNA withAUG or UUG start codon, and the eIF5-G31R variant (SUI5); chased with excess unlabeled TC for increasing periods of time; and the fraction of labeled Met-tRNA$_i$ bound to the PIC at each time-point determined by EMSA. (**B–D**) Representative plot of the fraction of [^{35}S]-Met-tRNA$_i$ incorporated into partial 48S complexes as a function of time for WT eIF2α, eIF2α-R55G-R57E and eIF2α-R55G-R57Q (B), from which mean rate constants (C) and end-points (D) (with SEMs) were calculated. Asterisks indicate significant differences between mutant and WT as judged by a two-tailed, unpaired Student's *t*-test (*$P < 0.05$; **$P < 0.01$).

and cannot be visualized in this experimental regime. Thus, the measured rate of TC dissociation in these assays largely reflects the proportion of complexes in the P$_{IN}$ state and the stability of that state with either an AUG or UUG in the P site (22,30). Because the Ssu$^-$ phenotypes of the eIF2α substitutions were observed in cells harboring a Sui$^-$ substitution in eIF2β or eIF5 (Figure 3A-B, respectively), we measured the off-rates of the mutant eIF2α TCs in the presence of the purified eIF5-G31R Sui$^-$ variant encoded by *SUI5.*

In contrast to experiments carried out with WT eIF2 and WT eIF5 (8,12), TC dissociates very little over the time course of the experiment from complexes containing either an AUG or UUG start codon when eIF5-G31R is used in place of WT eIF5 (Figure 5B, black symbols)—such that a dissociation rate constant (k_{off}) could be calculated only for the UUG complex, of ∼0.16 h^{-1} (Figure 5C, row 1)—which reflects stabilization of the closed/P$_{IN}$ state by this eIF5 variant (8). Importantly, the TC dissociation rates for the complexes assembled with either eIF2α-R55G/R57E or eIF2α-R55G/R57Q together with eIF5-G31R were increased for both the AUG and UUG mRNAs (Figure 5B, red and blue data points), by ∼4–5-fold for the mRNA(UUG) complexes where the change in rate constants could be calculated for both WT and mutant complexes (Figure 5C, col. 2; see representative data comparing eIF2α-R55G/R57E to WT eIF2α in Supplementary Figure S4, C versus B). The extent of TC dissociation at the last time point was also increased by both eIF2α variants, yielding lower proportions of the starting complexes at the end-points for the mutants compared to WT eIF2, particularly for UUG mRNA (Figure 5B and D). The fact that TC does not dissociate completely from the different PICs, even for the eIF2α mutant complexes formed with mRNA(UUG), is thought to reflect formation of a hyperstable state that is accessed from the closed/P$_{IN}$ conformation (30). Thus, the lowest proportions of starting complexes found at the

end-points for the UUG complexes formed with the eIF2α mutants (Figure 5D), indicates the smallest proportion of such complexes in the closed/P_{IN} conformation able to enter the non-dissociable hyperstable state observed among all reactions. Together, the results in Figure 5 indicate that both eIF2α double substitutions shift the partitioning of complexes away from the closed/P_{IN} conformation to the open/P_{OUT} state, consistent with their in vivo effects of reducing initiation at both UUG and poor-context AUG codons (Figures 3 and 4).

A charge-switch substitution of R53 in the eIF2α-D1 loop decreases discrimination against UUG and poor-context start codons *in vivo*

Comparing the structures of py48S-open and py48S-closed complexes revealed that R53 in the eIF2α-D1 loop interacts with the phosphodiester backbone of rRNA residue A906 in helix 23 in the open complex (Figure 6A). While R53 contacts the purine base, it appears to be too far away to contact the phosphodiester backbone of A_{906} in the closed complex (Figure 6B). This comparison suggested that electrostatic attraction of the R53 side-chain with the backbone of A_{906} might exclusively stabilize the open conformation. Accordingly, we asked whether R53 substitutions disrupting this interaction confer the dual Sui$^-$ and Gcd$^-$ phenotypes indicative of specific destabilization of the open conformation of the PIC (Figure 1B). Importantly, this expectation was fulfilled specifically for replacement of the basic side-chain of R53 with the acidic side-chain of glutamate in the R53E variant. The *R53E,* but not the *R53A* or *R53Q* mutations, conferred a Slg$^-$ phenotype on complete medium, particularly evident at 37°C (Figure 6C, row 3 versus rows 1–2 and 4); and also a Gcd$^-$ phenotype, as indicated by a marked increase in expression of a *GCN4-lacZ* reporter (harboring all four regulatory uORFs) under conditions of amino acid sufficiency that normally repress *GCN4* translation (Figure 6F, col. 3 versus col. 1). The *R53A* and *R53Q* mutations, by contrast, conferred only slight increases in *GCN4-lacZ* expression (Figure 6F, cols. 2 & 4 versus 3); and none of the substitutions in R54, R55, or R57 discussed above produced a significant derepression of *GCN4-lacZ* expression (Supplementary Figure S3) (Supplementary Table S4). The derepression of *GCN4* translation in Gcd$^-$ mutants occuring in the absence of amino acid starvation, and the attendant increase in eIF2α phosphorylation and decline in TC formation, signifies a reduced rate of TC recruitment to the open conformation of the PIC during the process of reinitiation on *GCN4* mRNA (4) (Figure 6D). Pronounced derepression of native *GCN4* mRNA in *R53E* cells was further indicated by increased resistance to sulfometuron methyl (SM), an inhibitor of Ile/Val synthesis that evokes eIF2α phosphorylation, induced synthesis of Gcn4, and elevated transcription of Ile/Val biosynthetic genes under Gcn4 control required for robust growth in medium containing SM. Cells lacking the eIF2α kinase Gcn2 are sensitive to SM owing to their inability to induce *GCN4* translation (Figure 6E, rows 1–2), and this SM-sensitivity can be suppressed by Gcd$^-$ mutations that constitutively derepress *GCN4* translation (4), as seen here for the *gcn2Δ sui2-R53E* double mutant (Figure 6E, row 4). *R53A* and *R53Q,* by contrast, confer only weak SM-resistance in *gcn2Δ* cells (Figure 6E, rows 3 & 5 versus 4), in accordance with their limited derepression of *GCN4-lacZ* expression noted above (Figure 6F). None of the R53 substitutions reduces expression of eIF2α (Figure 6G), consistent with a reduction in eIF2 function, not eIF2 expression, in recruitment of TC to the PIC in *sui2-R53E* cells.

A Sui$^-$ phenotype also was observed specifically for *sui2-R53E,* as indicated by an increase in the *HIS4-lacZ* UUG:AUG initiation ratio in otherwise WT cells (Figure 7A, col. 3 versus cols. 1–2 and 4). Moreover, decreased discrimination against poor-cognate AUG codons was conferred specifically by the *R53E* mutation as revealed by increased steady-state expression of eIF1 (Figure 7B, col. 3 versus cols. 1–2 and 4); and by increased expression of the *SUI1-lacZ* reporter with native, poor context relative to the $SUI1_{opt}$*-lacZ* reporter with optimum context. Whereas *R53E* reduced the $SUI1_{opt}$*-lacZ*/*SUI1-lacZ* ratio from ∼2.0 to ∼1.5, nearly WT ratios of ∼2.0 to ∼2.2 were observed for the *R53A* and *R53Q* mutations (Figure 7C, col. 3 versus cols. 1–2 and 4) (Supplementary Table S4). Finally, as shown in Figure 7D, we observed increased recognition of uAUG-1 (col. 6 versus 5) and a corresponding decrease in *GCN4-lacZ* expression (col. 2 versus 1, col. 4 versus 3) in the *R53E* mutant versus WT specifically for the *el.uORF1-GCN4-lacZ* reporters containing uAUG-1 in poor or weak context (rows 2–3 versus rows 1 and 4). (See also Supplementary Figure S5).

In summary, the Sui$^-$ R53E substitution reduces discrimination against a UUG start codon at *HIS4* and at the poor-context AUG start codons at *SUI1* and the elongated uORF1 of *el.uORF1-GCN4-lacZ*, both phenotypes consistent with an increased probability of the transition from the open, scanning state toward the closed conformation of the PIC, which increases its occurrence at poor initiation sites. Because TC loads most rapidly to the open complex (31), this interpretation can also account for the reduced rate of TC loading and attendant Gcd$^-$ phenotype of the *sui2-R53E* mutation. Such dual Sui$^-$/Gcd$^-$ phenotypes have been observed previously for Sui$^-$ mutations in eIF1, eIF1A, and eIF2β that also appear to specifically disfavor the open conformation of the PIC (9,10,12,32). Considering that marked Sui$^-$/Gcd$^-$ phenotypes are conferred by the Glu substitution, but not Ala or Gln substitutions of R53, it seems likely that introducing a negative charge at this position introduces electrostatic repulsion with the phosphodiester backbone of rRNA specifically in the open complex in which R53 contacts the backbone of A_{906} in helix 23 (Figure 6A and B).

In vitro evidence that eIF2α-R53E reduces the rate of TC loading to the open conformation while increasing transition to the closed state with more tightly bound TC

As noted above, the Gcd$^-$ phenotype of *sui2-R53E* indicates a reduced rate of TC loading to the open conformation of the PIC during the process of reinitiation on *GCN4* mRNA *in vivo* (Figure 6D–F). To support this interpretation biochemically, we measured the kinetics of TC binding to 40S·eIF1A·eIF1·mRNA complexes assembled with either WT eIF2 or eIF2 harboring the eIF2α-R53E variant

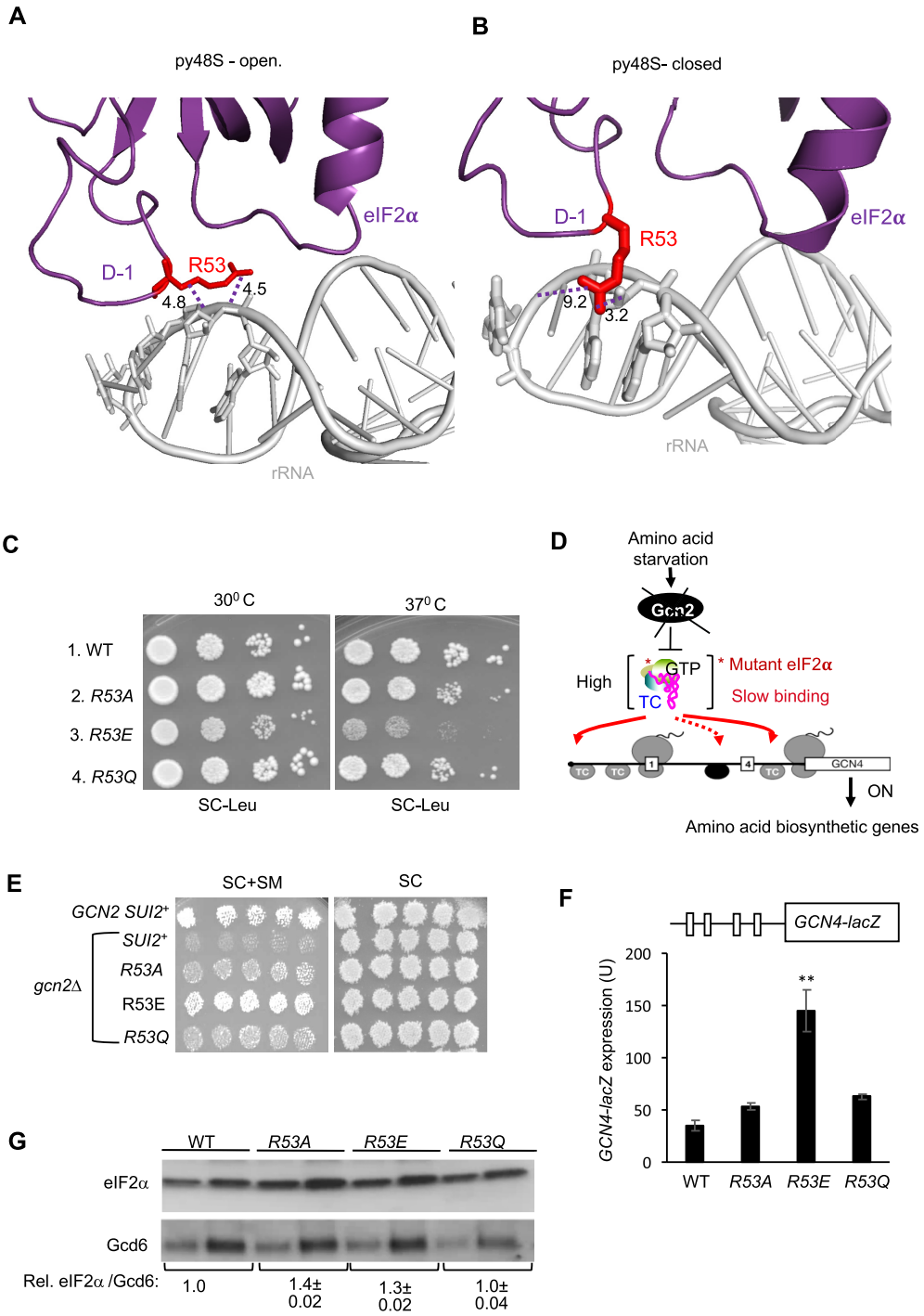

Figure 6. Substitution R53E in the eIF2α-D1 loop derepresses *GCN4-lacZ* expression *in vivo*. (**A**, **B**) Interactions between eIF2α-R53 and rRNA helix 23 in the py48S-open (A) and py48S-closed (B) states of the PIC (10). eIF2α is shown in purple, R53 shown as sticks in red, and rRNA in grey. (**C**) Ten-fold serial dilutions of H2507 derivatives with the indicated *SUI2* alleles were spotted on synthetic complete medium lacking leucine (SC-Leu) and incubated at 30°C or 37°C for 2–3 days. (**D**) In otherwise WT *gcn2Δ* cells (lacking kinase Gcn2), *GCN4* translation remains repressed in starvation conditions because of high TC levels that ensure that all post-termination 40S complexes that resume scanning after translating uORF1 rebind TC before reaching uORF4 and are evicted from the mRNA after uORF4 translation. A mutation in eIF2α (red asterisk) that lowers the rate of TC loading even at the high TC levels in *gcn2Δ* cells allows a fraction of scanning 40S complexes to rebind TC only after bypassing uORF4 (solid vs. dotted red arrows on right) and then reinitiate at the *GCN4* AUG instead, derepressing *GCN4* translation. (**E**) Parental *GCN2*$^{+}$ *SUI2*$^{+}$ strain and derivatives of *gcn2Δ* strain with the indicated *SUI2* alleles were replica-printed to synthetic complete medium lacking Leu (SC) or SC lacking Leu, Ile and Val and containing 0.3 ug/ml SM (SC + SM) and incubated for 3 days. (**F**) Transformants of H2507 containing the indicated *SUI2* alleles and WT *GCN4-lacZ* reporter (depicted schematically) on plasmid p180 were assayed for β-galactosidase activities as in Figure 2D. Mean expression levels and SEMs calculated from six transformants of each strain are plotted. Asterisk indicate significant differences between mutant and WT as judged by a two-tailed, unpaired Student's *t*-test (**$P < 0.01$). **(G)** Derivatives of *sui2Δ* strain H2507 containing the indicated *SUI2* alleles were cultured in SD supplemented with Trp and Ura at 30°C to A_{600} of ∼1.0, and WCEs were subjected to western blot analysis using antibodies against eIF2α and Gcd6 (loading control), all as in Figure 2E.

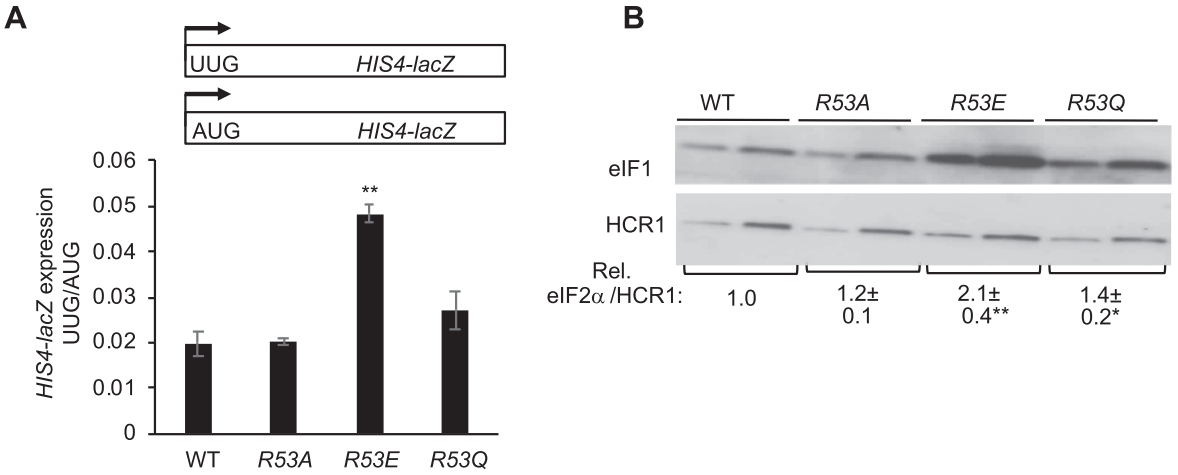

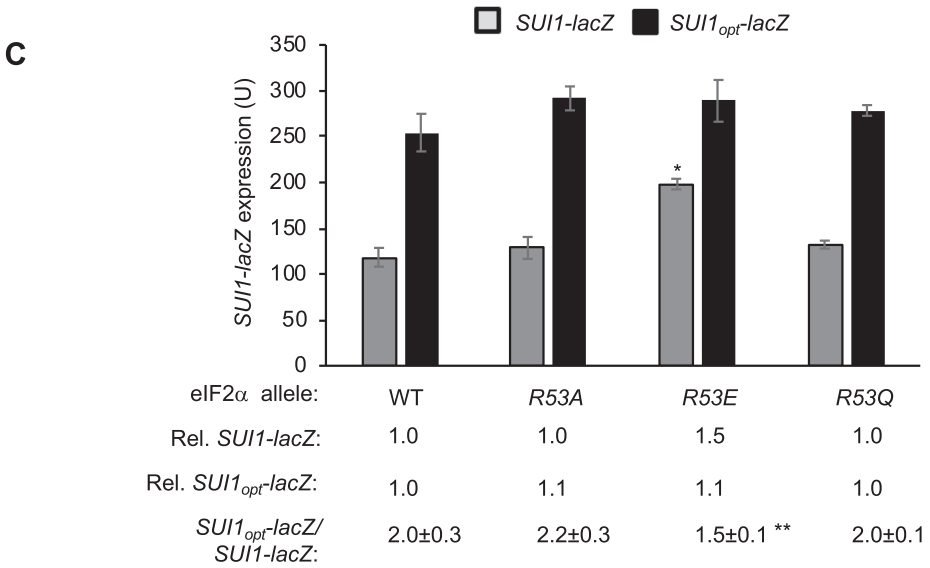

D

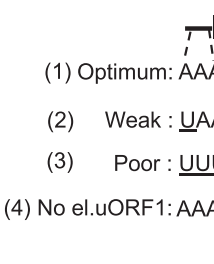

	GCN4-lacZ expression(U)		% translating GCN4-lacZ		% translating el. uORF1	
	(1) WT	(2) R53E	(3) WT	(4) R53E	(5) WT	(6) R53E
(1) Optimum: AAA AUG AUG	7±0.7	28±0.4**	0.4	1.7	99.6	98.3
(2) Weak : UAA AUG	118±11	79±5**	8	5	92	95
(3) Poor : UUUAUG	387±43	200±52*	26	12	74	88
(4) No el.uORF1: AAA AGC GCN4-lacZ AUG	1485±200	1621±250	>99	>99	<1	<1

Figure 7. Substitution R53E in the eIF2α-D1 loop decreases discrimination against UUG start codons and AUG codons in suboptimal contexts *in vivo*. (**A**) Derivatives of *sui2Δ* strain H2507 containing the indicated *SUI2* alleles, each harboring the appropriate *HIS4-lacZ* reporter with UUG or AUG start codons, were analyzed as in Figure 2D. (**B**) Derivatives of *sui2Δ* strain H2507 containing the indicated *SUI2* alleles were cultured in SD supplemented with Trp and Ura at 30°C to A_{600} of ∼1.0, and WCEs were subjected to western blot analysis using antibodies against eIF1 and Hcr1 (as loading control). Two amounts of each extract differing by a factor of two were loaded in successive lanes. eIF2α western signals were normalized to those for Hcr1 and mean values (±SEM) were calculated from three biological replicates. (**C**) The same strains as in (A) but harboring sc plasmids (pPMB24 or pPMB25) with *SUI1-lacZ* fusions with native suboptimal ($_{-3}$CGU$_{-1}$) or optimum ($_{-3}$AAA$_{-1}$) AUG contexts were cultured and assayed for β-galactosidase activities as in Figure 2D and analyzed as in Figure 4C. (**D**) Transformants of H2507 harboring WT *SUI2*, *sui2-R53E* and the four *GCN4-lacZ* reporters described in Figure 4D were analyzed as described in Figure 4D and Supplementary Figure S2. Asterisks indicate significant differences between mutant and WT as judged by a two-tailed, unpaired Student's *t*-test (*$P < 0.05$; **$P < 0.01$).

using the gel mobility shift assay described above. WT TC preassembled with [^{35}S]-Met-tRNA$_i$ was added to initiate the reactions, which were terminated at each time point with excess unlabeled TC (Figure 8A). The pseudo-first-order rate constants (k_{obs}) were measured at different 40S concentrations to obtain the second-order rate constant (k_{on}) (22). Compared to WT eIF2, the variant with eIF2α-R53E confers an ∼2-fold decrease in k_{on} for mRNA(AUG) (Figure 8B and C). These findings support the notion that R53E destabilizes the open conformation of the PIC and favors the transition to the closed state, and that the reduced occupancy of the open complex impairs TC loading to this conformation of the PIC.

A second consequence of increasing the transition to the closed conformation predicted for the eIF2α-R53E variant is a decrease in the dissociation rate of TC from PICs reconstituted with mRNA(UUG). To test this prediction, we measured the kinetics of TC dissociation using the same assay described above except that eIF5-G31R was omitted, as the influence of this Sui$^-$ variant was not relevant here (Figure 8D. The results showed that eIF2α-R53E reduced both the off-rate and extent of TC dissociation at UUG codons (Figure 8E-F, ovals, red vs. black; representative data in Supplementary Figure S6), as expected from increased occupancy of the closed/P$_{IN}$/hyperstable states from which TC dissociates more slowly relative to the open/P$_{OUT}$ conformation with a mismatched UUG:anticodon helix in the P site. A significant, but much less pronounced stabilization of TC binding was also observed for mRNA(AUG) complexes (Figure 8E, F, squares, red versus black). The relatively greater stabilization of TC at UUG versus AUG in these experiments is consistent with the increased UUG:AUG initiation ratio observed for this eIF2α substitution *in vivo* (Figure 7A). Thus, the biochemical data indicate a specific destabilization of the open conformation, with attendant reduction in the rate of TC loading and a shift towards the closed conformation with more tightly bound TC, on perturbing contact of eIF2α-R53 with rRNA residue A_{906} in the open complex.

DISCUSSION

In this report, we provide evidence from a combination of genetics and biochemistry that conserved Arg residues R55 and R57 in a loop present in domain D-1 of eIF2α play an important role in stabilizing the closed/P$_{IN}$ conformation of the 48S PIC and, as such, promote efficient initiation at near-cognate start codons and AUGs in poor Kozak context. The cryo-EM structures of py48S complexes in open or closed conformation revealed that R55/R57 interact with the Kozak context nucleotides in mRNA exclusively in the py48S-closed structure, which contains mRNA and Met-tRNA$_i$ tightly locked into the mRNA binding cleft and P site, respectively, and thought to depict the PIC conformation during AUG recognition (10). These contacts are absent in the py48S-open structure owing to upward displacement of the 40S head away from the 40S body and movements of the eIF2α domains relative to the tRNA$_i$, mRNA and other PIC components (10) (Figure 2A-B). Based on the structural data, we hypothesized that the R55/R57 contacts with mRNA specifically stabilize the closed/P$_{IN}$ state, and might also mediate the stimulatory effects of an A nucleotide at the –3 position, to promote selection of AUG start codons in favorable context. Our results support the role of R55/R57 in stabilizing the closed/P$_{IN}$ state; however they do not indicate a role for these residues in recognizing optimum Kozak context.

Our genetic analyses showed that substitutions of R55 and R57 increase discrimination against a UUG start codon at *HIS4* and thereby decrease the UUG:AUG initiation ratio for a *HIS4-lacZ* reporter in cells harboring Sui$^-$ mutations in eIF2β (*SUI3-2*) or eIF5 (*SUI5) in vivo*, conferring the Ssu$^-$ phenotype. These substitutions also increase discrimination against the poor-context AUG codon in *SUI1* mRNA to reduce eIF1 expression (Supplementary Table S4). Consistent with the latter, they increase leaky scanning of uAUG-1 at *GCN4* uORF1 with a greater quantitative effect when uAUG-1 resides in poor versus optimal context. These results do not support a role for R55/R57 in recognizing a favorable purine nucleotide at the –3 position of the Kozak context, since according to that model substituting these residues should preferentially impair recognition of AUGs with A/G at –3 and have little or no effect with U/C at this position—the opposite of our findings. Instead, these genetic data closely resemble those we described previously for Ssu$^-$ substitutions in the NTT of eIF1A (13) predicted to disrupt direct interactions of the NTT with the AUG:anticodon helix of Met-tRNA$_i$ and adjacent mRNA nucleotides exclusively in the closed PIC conformation (10,33). Two such eIF1A substitution (K16D and R16P) destabilized the closed/P$_{IN}$ conformation of 48S PICs *in vitro* when reconstituted with mRNA harboring a UUG start codon—the same biochemical defect observed here for the eIF2α R55G/R57E and R55G/R57Q substitutions. Accordingly, it appears that interactions of WT residues R55 and R57 with the mRNA upstream of the start codon functionally cooperate with eIF1A-NTT interactions to stabilize the closed/P$_{IN}$ conformation of the PIC (Supplementary Figure S7A), such that substitutions in these residues reduce the likelihood of rearrangement from the open to closed state at UUG start codons, for the Ssu$^-$ phenotype (Supplementary Figure S7B).

In our genetic experiments, we found that the R55G/R57E and R55G/R57Q eIF2α substitutions both confer a much larger increase in leaky scanning of uAUG-1 in poor context compared to optimal Kozak context (Figure 4D). This finding ostensibly suggests that these substitutions preferentially discriminate against poor versus optimal start codons; however we examined this assumption more rigorously using thermodynamic considerations to evaluate our results with the *el.uORF1-GCN4-lacZ* reporter (Figure 4D), which provide the proportion of scanning ribosomes that either initate at uAUG-1 or continue scanning and use the *GCN4* AUG instead. As explained fully in the Supplementary Discussion, we assumed that recognition of *el.-uORF1* is dictated by a dynamic equilibrium between the open and closed states of the 48S PIC at uAUG-1, and calculated the equilibrium constant ($K_{closed/open}$) as the ratio of the proportion of ribosomes that translate *el.-uORF1* (taken from Figure 4D, cols. 7–9) to that which bypass uAUG-1 and translate *GCN4-lacZ* (Figure 4D, cols. 4–6); and we determined

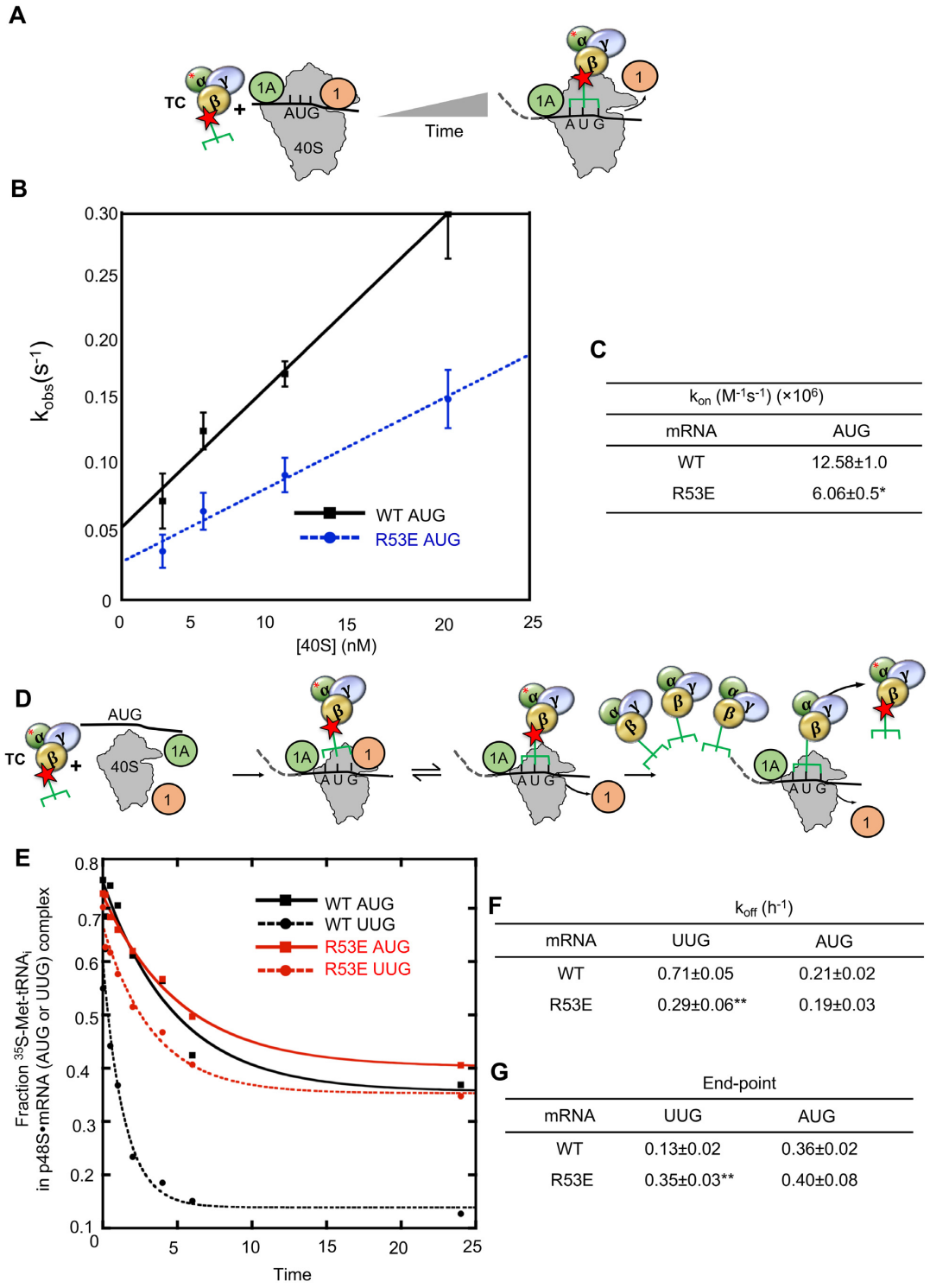

Figure 8. Substitution R53E in the eIF2α-D1 loop reduces the rate of TC binding but enhances the closed/P_{IN} conformation of py48S PICs at UUG codons *in vitro*. (**A**) Schematic for measurement of TC association kinetics. TC preassembled with [^{35}S]-Met-tRNA$_i$ was mixed with pre-formed 40S·eIF1A·eIF1·mRNA complexes, incubated for increasing times, and reactions were terminated at each time-point with a chase of excess unlabeled TC. The fraction of labeled Met-tRNA$_i$ bound to the partial 48S complexes at each time-point was determined by EMSA. The pseudo-first-order rate constant (k_{obs}) was measured at different 40S concentrations to obtain the second order rate constant (k_{on}). (**B**, **C**) Determination of k_{on} values as described in (A) for TCs assembled with eIF2 containing either WT eIF2α or mutant eIF2α-R53E and mRNA(AUG). Mean k_{obs} values determined from three independent experiments at each 40S concentration. The resuting mean k_{obs} values are plotted against each 40S concentration with error bars representing SEM (B) k_{obs} values from each of three independent experiments were plotted against 40S concentration in order to calculate k_{on}, and mean K_{on} values (with SEMs) are shown (C). (**D**, **G**) TC dissociation kinetics were determined for TCs assembled with [^{35}S]-Met-tRNA$_i$ and eIF2 containing either WT eIF2α or mutant eIF2α-R53E, exactly as described in Figure 5A–D. (C, F, G) Asterisks indicate significant differences between mutant and WT as judged by a two-tailed, unpaired Student's *t*-test (*$P < 0.05$; **$P < 0.01$).

this constant for each of the three contexts of uAUG-1 examined (optimum, weak, and poor), designating them K_{opt}, K_{weak} and K_{poor}. The resulting constants were then used to calculate the differences in free energy between the closed and open states ($\Delta G^{\circ}_{closed\text{-}open}$) at uAUG-1 for optimal, weak, and poor contexts. Performing this calculation for both the WT and *R55G/R57E* strains yielded the change in the $\Delta G^{\circ}_{closed\text{-}open}$ values between mutant and WT ($\Delta\Delta G^{\circ}_{mutant\text{-}WT}$) for each uAUG-1 context. Interestingly, the $\Delta\Delta G^{\circ}_{mutant\text{-}WT}$ values were similar for all three contexts, of between ~0.5 and 1.0 kcal mol^{-1}. This finding implies that the *R55G/R57E* mutations decrease the stability, and thus increase the free energy, of the closed complex by nearly the same amount regardless of the Kozak context. According to our thermodynamic model, the fact that *R55G/R57E* produce a much smaller decrease in the proportion of scanning ribosomes that recognize uAUG-1 in optimum versus poor context simply reflects the lower free energy of the closed state with optimum context, which remains relatively low even with the increased free energy conferred by the eIF2α mutations, with the result that K_{poor} remains relatively high and the majority of ribosomes still utilize uAUG-1 in poor context in the mutant cells (see Supplementary Discussion for further details). This analysis implies that R55 and R57 do not discriminate between different context nucleotides but, rather, destabilize the closed/P_{IN} state equally regardless of the Kozak context. If the same situation applies to different start codons, this would also explain our biochemical results indicating that R55G/R57E and R55G/R57Q destabilize the closed/P_{IN} conformation of the PIC even with an AUG codon in the mRNA, but to a lesser degree than observed with a UUG start codon (Figure 5B–D).

Whereas R55 and R57 contact the mRNA only in the py48S-closed PIC, the nearby loop residue R53 interacts with the phosphodiester backbone of rRNA helix 23 exclusively in py48S-open (10), which is consistent with a role in preferentially stabilizing the open, scanning conformation of the PIC (Supplementary Figure S7A). Supporting this idea, we found that Glu, but not Ala or Gln substitutions of this residue conferred the dual Gcd$^-$ and Sui$^-$ phenotypes characteristic of mutations in eIF1 or eIF1A that preferentially destabilize the open conformation and shift the equilibrium towards the closed state, reducing the rate of TC loading to the open complex to derepress *GCN4* translation (Gcd$^-$ phenotype) and also increasing the probability of initiating at near-cognate UUG codons (Sui$^-$ phenotype) (Supplementary Figure S7C) (Supplementary Table S4). Consistent with the Gcd$^-$ phenotype, the R53E substitution reduced the on-rate of TC binding to reconstituted PICs. At the same time, R53E decreased the off-rate of TC at UUG start codons *in vitro*, in accordance with its *in vivo* Sui$^-$ phenotype. In addition to relaxing discrimination against UUG start codons, *R53E* also increased recognition of the poor-context AUG codons in *SUI1* mRNA (Supplementary Table S4) and at elongated uORF1 of the *el.-uORF1-GCN4-lacZ* reporter with uAUG-1 in poor context. In decreasing discrimination against poor start codons, *R53E* has the opposite effects on initiation fidelity compared to the hyperaccuracy phenotypes conferred by the R55 and R57 substitutions.

Taken together, our findings indicate that the different Arg residues in the loop of eIF2α D-1 have opposing roles in scanning and start codon selection. The R53 interaction with rRNA in helix 23, found exclusively in the open complex, acts to promote scanning; whereas the R55/R57 contacts with mRNA confined to the closed complex help to arrest scanning and enable start codon recognition (Supplementary Figure S7A). Owing to the inherently less stable closed complexes formed at near-cognate versus AUG start codons, disrupting these interactions increase (for R53E) or decrease (for R55/R57 substitutions) the frequency of UUG initiation *in vivo*. Our thermodynamic analysis of the effects of the *R55G/R57E* mutations on leaky scanning of *el.uORF1*, suggest that poor context surrounding AUG codons also destabilizes the closed conformation of the PIC, such that these eIF2α mutations confer a greater reduction in the frequency of initiation at poor-context versus optimal-context AUG codons.

Similar to our findings here, we showed previously that distinct interactions of a different region of eIF2α D-1 with the 40S protein uS7 are restricted to either py48S-open or py48S-closed and exert opposing effects on the accuracy of start codon recognition (25). It is remarkable that two different surfaces of eIF2α D1, one interacting with mRNA and the other with uS7, both undergo a remodeling of their respective interactions in the transition from open to closed states of the PIC to promote first scanning by the open conformation, and then start codon selection by the closed complex. Moreover, the eIF2α-D1 interactions with mRNA described here can be added to a list of molecular interactions that specifically stabilize the open or closed state of the PIC, including the eIF2α/uS7 interactions just mentioned, contacts of eIF1 and eIF2β with one another and with $tRNA_i$ (10–12), eIF1A–NTT interactions with mRNA and $tRNA_i$ (13), and eIF5-NTD contacts with $tRNA_i$ (3). Presumably, the relative strengths of these contacts in the open or closed states have been tuned during evolution to yield the most adaptive frequencies of initiation at poor versus optimum initiation sites.

SUPPLEMENTARY DATA

Supplementary Data are available at NAR Online.

ACKNOWLEDGEMENTS

We thank Jinsheng Dong, Fan Zhang, Jagpreet Nanda, Laura Marler and Jon Lorsch for advice and assistance in using the yeast reconstituted system, Henry Zhang, Fujun Zhou and Shardul Kulkarni for assistance in data analysis, and all members of our laboratory and those of Jon Lorsch, Tom Dever and Nick Guydosh for many valuable suggestions.

FUNDING

Intramural Research Program of the National Institutes of Health. Funding for open access charge: Intramural Research Program of the National Institutes of Health.
Conflict of interest statement. None declared.

REFERENCES

1. Hinnebusch,A.G. (2014) The scanning mechanism of eukaryotic translation initiation. *Annu. Rev. Biochem.*, **83**, 779–812.
2. Hinnebusch,A.G. (2017) Structural insights into the mechanism of scanning and start codon recognition in eukaryotic translation initiation. *Trends Biochem. Sci.*, **42**, 589–611.
3. Llacer,J.L., Hussain,T., Saini,A.K., Nanda,J.S., Kaur,S., Gordiyenko,Y., Kumar,R., Hinnebusch,A.G., Lorsch,J.R. and Ramakrishnan,V. (2018) Translational initiation factor eIF5 replaces eIF1 on the 40S ribosomal subunit to promote start-codon recognition. *Elife*, **7**, e39273.
4. Hinnebusch,A.G. (2005) Translational regulation of GCN4 and the general amino acid control of yeast. *Annu. Rev. Microbiol.*, **59**, 407–450.
5. Donahue,T. (2000) In: Sonenberg,N., Hershey,J.W.B. and Mathews,M.B. (eds). *Translational Control of Gene Expression*. Cold Spring Harbor Laboratory Press, NY, pp. 487–502.
6. Martin-Marcos,P., Cheung,Y.N. and Hinnebusch,A.G. (2011) Functional elements in initiation factors 1, 1A, and 2beta discriminate against poor AUG context and non-AUG start codons. *Mol. Cell. Biol.*, **31**, 4814–4831.
7. Ivanov,I.P., Loughran,G., Sachs,M.S. and Atkins,J.F. (2010) Initiation context modulates autoregulation of eukaryotic translation initiation factor 1 (eIF1). *Proc. Natl. Acad. Sci. U.S.A.*, **107**, 18056–18060.
8. Martin-Marcos,P., Nanda,J.S., Luna,R.E., Zhang,F., Saini,A.K., Cherkasova,V.A., Wagner,G., Lorsch,J.R. and Hinnebusch,A.G. (2014) Enhanced eIF1 binding to the 40S ribosome impedes conformational rearrangements of the preinitiation complex and elevates initiation accuracy. *RNA*, **20**, 150–167.
9. Martin-Marcos,P., Nanda,J., Luna,R.E., Wagner,G., Lorsch,J.R. and Hinnebusch,A.G. (2013) beta-hairpin loop of eIF1 mediates 40S ribosome binding to regulate initiator tRNAMet recruitment and accuracy of AUG selection in vivo. *J. Biol. Chem.*, **288**, 27546–27562.
10. Llacer,J.L., Hussain,T., Marler,L., Aitken,C.E., Thakur,A., Lorsch,J.R., Hinnebusch,A.G. and Ramakrishnan,V. (2015) Conformational differences between open and closed states of the eukaryotic translation initiation complex. *Mol. Cell*, **59**, 399–412.
11. Thakur,A. and Hinnebusch,A.G. (2018) eIF1 Loop 2 interactions with Met-tRNAi control the accuracy of start codon selection by the scanning preinitiation complex. *Proc. Natl. Acad. Sci. U.S.A.*, **115**, E4159–E4168.
12. Thakur,A., Marler,L. and Hinnebusch,A.G. (2018) A network of eIF2beta interactions with eIF1 and Met-tRNAi promotes accurate start codon selection by the translation preinitiation complex. *Nucleic Acids Res.*, **47**, 2574–2593.
13. Martin-Marcos,P., Zhou,F., Karunasiri,C., Zhang,F., Dong,J., Nanda,J., Kulkarni,S.D., Sen,N.D., Tamame,M., Zeschnigk,M. *et al.* (2017) eIF1A residues implicated in cancer stabilize translation preinitiation complexes and favor suboptimal initiation sites in yeast. *Elife*, **6**, e31250.
14. Kozak,M. (1999) Initiation of translation in prokaryotes and eukaryotes. *Gene*, **234**, 187–208.
15. Hinnebusch,A.G. (2011) Molecular mechanism of scanning and start codon selection in eukaryotes. *Microbiol. Mol. Biol. Rev.*, **75**, 434–467.
16. Pisarev,A.V., Kolupaeva,V.G., Pisareva,V.P., Merrick,W.C., Hellen,C.U. and Pestova,T.V. (2006) Specific functional interactions of nucleotides at key −3 and +4 positions flanking the initiation codon with components of the mammalian 48S translation initiation complex. *Genes Dev.*, **20**, 624–636.
17. Moehle,C.M. and Hinnebusch,A.G. (1991) Association of RAP1 binding sites with stringent control of ribosomal protein gene transcription in *Saccharomyces cerevisiae*. *Mol. Cell. Biol.*, **11**, 2723–2735.
18. Reid,G.A. and Schatz,G. (1982) Import of proteins into mitochondria. Yeast cells grown in the presence of carbonyl cyanide m-chlorophenylhydrazone accumulate massive amounts of some mitochondrial precursor polypeptides. *J. Biol. Chem.*, **257**, 13056–13061.
19. Nanda,J.S., Cheung,Y.N., Takacs,J.E., Martin-Marcos,P., Saini,A.K., Hinnebusch,A.G. and Lorsch,J.R. (2009) eIF1 controls multiple steps in start codon recognition during eukaryotic translation initiation. *J. Mol. Biol.*, **394**, 268–285.
20. Olsen,D.S., E.M.,S., Mathew,A., Zhang,F., Krishnamoorthy,T., Phan,L. and Hinnebusch,A.G. (2003) Domains of eIF1A that mediate binding to eIF2, eIF3 and eIF5B and promote ternary complex recruitment *in vivo*. *EMBO J.*, **22**, 193–204.
21. Acker,M.G., Kolitz,S.E., Mitchell,S.F., Nanda,J.S. and Lorsch,J.R. (2007) Reconstitution of yeast translation initiation. *Methods Enzymol.*, **430**, 111–145.
22. Kolitz,S.E., Takacs,J.E. and Lorsch,J.R. (2009) Kinetic and thermodynamic analysis of the role of start codon/anticodon base pairing during eukaryotic translation initiation. *RNA*, **15**, 138–152.
23. Boeke,J.D., Trueheart,J., Natsoulis,G. and Fink,G.R. (1987) 5-fluoroorotic acid as a selective agent in yeast molecular genetics. *Methods Enzymol.*, **154**, 164–175.
24. Huang,H., Yoon,H., Hannig,E.M. and Donahue,T.F. (1997) GTP hydrolysis controls stringent selection of the AUG start codon during translation initiation in *Saccharomyces cerevisiae*. *Genes Dev.*, **11**, 2396–2413.
25. Visweswaraiah,J. and Hinnebusch,A.G. (2017) Interface between 40S exit channel protein uS7/Rps5 and eIF2alpha modulates start codon recognition in vivo. *Elife*, **6**, e22572.
26. Visweswaraiah,J., Pittman,Y., Dever,T.E. and Hinnebusch,A.G. (2015) The beta-hairpin of 40S exit channel protein Rps5/uS7 promotes efficient and accurate translation initiation in vivo. *Elife*, **4**, e07939.
27. Dong,J., Aitken,C.E., Thakur,A., Shin,B.S., Lorsch,J.R. and Hinnebusch,A.G. (2017) Rps3/uS3 promotes mRNA binding at the 40S ribosome entry channel and stabilizes preinitiation complexes at start codons. *Proc. Natl. Acad. Sci. U.S.A.*, **114**, E2126–E2135.
28. Zur,H. and Tuller,T. (2013) New universal rules of eukaryotic translation initiation fidelity. *PLoS Comput. Biol.*, **9**, e1003136.
29. Grant,C.M., Miller,P.F. and Hinnebusch,A.G. (1994) Requirements for intercistronic distance and level of eIF-2 activity in reinitiation on GCN4 mRNA varies with the downstream cistron. *Mol. Cell. Biol.*, **14**, 2616–2628.
30. Dong,J., Munoz,A., Kolitz,S.E., Saini,A.K., Chiu,W.L., Rahman,H., Lorsch,J.R. and Hinnebusch,A.G. (2014) Conserved residues in yeast initiator tRNA calibrate initiation accuracy by regulating preinitiation complex stability at the start codon. *Genes Dev.*, **28**, 502–520.
31. Passmore,L.A., Schmeing,T.M., Maag,D., Applefield,D.J., Acker,M.G., Algire,M.A., Lorsch,J.R. and Ramakrishnan,V. (2007) The eukaryotic translation initiation factors eIF1 and eIF1A induce an open conformation of the 40S ribosome. *Mol. Cell*, **26**, 41–50.
32. Saini,A.K., Nanda,J.S., Lorsch,J.R. and Hinnebusch,A.G. (2010) Regulatory elements in eIF1A control the fidelity of start codon selection by modulating tRNA(i)(Met) binding to the ribosome. *Genes Dev.*, **24**, 97–110.
33. Hussain,T., Llácer,J.L., Fernández,I.S., Munoz,A., Martin-Marcos,P., Savva,C.G., Lorsch,J.R., Hinnebusch,A.G. and Ramakrishnan,V. (2014) Structural changes enable start codon recognition by the eukaryotic translation initiation complex. *Cell*, **159**, 597–607.
34. Hinnebusch,A.G. and Lorsch,J.R. (2012) The mechanism of eukaryotic translation initiation: new insights and challenges. *Cold Spring Harb. Perspect. Biol.*, **4**, a011544.
35. Nanda,J.S., Saini,A.K., Munoz,A.M., Hinnebusch,A.G. and Lorsch,J.R. (2013) Coordinated movements of eukaryotic translation initiation factors eIF1, eIF1A, and eIF5 trigger phosphate release from eIF2 in response to start codon recognition by the ribosomal preinitiation complex. *J. Biol. Chem.*, **288**, 5316–5329.